NMR and molecular dynamics structural investigations of *Manduca sexta* stress response peptides and *Anopheles gambiae* ecdysis triggering hormone.

by

Hawa Dembele

A THESIS

submitted in partial fulfillment of the requirements for the degree

Department of Biochemistry and Molecular Biophysics
College of Arts and Sciences

KANSAS STATE UNIVERSITY
Manhattan, Kansas

2021

Approved by:

Major Professor
Om Prakash

Copyright

© Hawa Dembele 2021.

Abstract

Stress-responsive peptides (SRPs) represent a largely unexplored group of peptides within the class of Insecta that regulate cell chemotaxis, proliferation, and anti-microbial gene expression. The diverse functions of these peptides led us to undertake structure-activity relationship studies of Stress-Response Peptides 1 and 2 (SRP-1 and -2) secreted by the lepidopteran *Manduca sexta* in response to biotic and abiotic stressors. Mature SRP-1 and -2 contain 25 residues and one disulfide linkage between residues C8 and C19. We have previously determined the solution structure of SRP-1/2 using 2D ^{1}H-^{1}H NMR spectroscopy and nuclear Overhouser enhancement (NOE) derived distance constraints. The NMR structural studies showed a large number of NOE contacts between the side chain of residue 12 and the side chains of residues C8, P9 and C19 in both peptides. The high density of long-range NOE contacts for this residue (Y12 for SRP-1, and R12 for SRP-2) are similar to those of residue Y11 present in the Plasmocyte Spreading Peptide (PSP) of *Pseudopulsia includes* and Paralytic peptide (PP) from *Manduca sexta*. Earlier, studies suggested that residue Y11 plays an important role in the stabilization of PSP and PP structures. It was also observed that replacement of Y11 in PSP substantially reduced the biological activity in comparison to wild type. To better understand the role of residue Y12 and R12 in maintaining the structural stability of SRP-1 and SRP-2, we have conducted Molecular Dynamics Studies of SRP-1 and -2 wild type and select mutants (Y/R12A, Y/R12E, R12K, Y12R and R12Y). Our results indicate a more drastic increase in flexibility of the core region for all SRP1 mutants while the SRP-2 mutants showed dynamic characteristics relatively similar to wild type. Subsequent secondary structural characteristics analyses suggest that the increase in flexibility observed in SRP-1 mutants could be due to a drop in Beta strand

formation propensity between residues Y12-R15 and F18-P21. Alpha helical propensity analyses of SRP-2 and mutants show a drastic change in alpha helix formation for SRP-2 mutants in comparison to wild type. This discrepancy in N-terminal alpha helix formation could be explained by a decrease in salt-bridge formation propensity for contacts D22-K7, and D24-K7 in SRP-2. Overall, our mutational analyses of SRP-1 and SRP-2 show that mutations at the embedded position have a more drastic impact on the rigidity and flexibility of SRP-1 than SRP-2.

Infections by mosquito-borne diseases represent one of the leading causes of death in third world countries. The rapid progression of resistance to conventional insecticide causes a significant threat to the highly efficient preventive methods currently in place. Deletion of the Ecdysis Triggering Hormone (ETH) encoding gene has been proven to result in fatal deficits in *Drosophila*. Our current study explores the impact of point mutations on the structural integrity and function of ETH from the African Malaria Mosquito, *Anopheles gambiae* (AgETH). We herein have determined the solution structure of AgETH1 using 2D ^{1}H-^{1}H Nuclear Magnetic Resonance (NMR) spectroscopy and Nuclear Overhauser Effect (NOE) derived constraints. Our findings showed that the 17 amino acid peptide contains a short alpha helix between residues 3S and 11S. ETH is specifically characterized by the C-terminal motif PRXamide and sequence alignments of ETH peptides from several organisms suggests that the heavily conserved C-terminal PRXamide motif is critical for receptor activation. Seven mutations at various heavily conserved residue positions were performed to assess their subsequent effect on receptor activation by AgETH1. Our results show retention of peptide activity for mutants lacking the N-terminal region but containing the two highly conserved Lysine residues. These results suggest that the presence of the alpha helical structure observed for AgETH1 WT may be important for

receptor activation. Furthermore, the activity assay results show that one of the highly conserved lysine residues (K12) may play a more critical role than the other (K9). Understanding peptide-receptor binding of AgETH1 will be a significant assistance for the development of insecticidal compounds that disrupt the ecdysis triggering hormone system that is a crucial component of larvae development specific to the insect species.

Table of Contents

List of Figures

Chapter 1

Chapter 2

List of Tables

Acknowledgements

I would like to thank my major professor, Dr. Om Prakash for all his support and mentorship throughout this process. Thank you for always providing insightful feedback on my work and for encouraging me to work harder to achieve my goals.

I would also like to thank my committee members, Dr. Yoonseong Park, and Dr. Ho Leung Ng for their time and effort in providing guidance as I collected the CD and functional assay data. And of course, I would like to thank them for their valuable feedback on manuscripts, presentations, and this thesis.

I want to thank all members, present and former, of the NMR lab. In particular, I would like to thank Dr. Indrani Pal, Dr. Lynn Schrag and Dr. Alvaro Herrera for taking me in as their mentee and for teaching me all I know today. Their excellent mentorship and immense patience helped be become a better scientist and overall person. I also want to thank Ng lab member Ye Zhou, for all her help with homology modeling and all her advice when it comes to computational methods. Finally, I want to thank Rupinder from the Park lab for helping me run and set up the activity assays with the AgETH project.

Finally, I would like to thank my friends and family, those close by and those far away, for their support and encouragement, and Allah swt for equipping me with the strength to seek challenges and surmount them.

Dedication

To my parents, Nango Dembele and Bintou Dembele, for believing in my dreams before I was even born. For providing me with not only the material means, but also the emotional support that allowed me to pursue my dreams. This thesis is not only a reflection of the work I have accomplished in the lab, but it is reflection of the continued support of you both. This thesis is as much mine as it is yours. Thank you, and I love you.

To my sister, Fatoumata Dembele, for always being here to listen to my rants and complaints when things got difficult. For always supporting my goals and dreams, no matter how big or unrealistic. For always inspiring me to reach higher, to never take no for an answer, and to keep striving for a better version of myself. Without you, none of this would be possible, thank you for being a sister when I need advice, a mom when I need comforting, and a best friend when I need a confidant. This work is as much mine as it is yours and I am so thankful to have you in my life. Thank you, and I love you.

Chapter 1 - Structural Characterization of *Manduca sexta* Stress Responsive Peptides.

1.1. Introduction

Stress-responsive peptides (SRPs) are a class of cytokines that mediate innate immune responses in insects. The first SRP-like molecule identified was isolated from the armyworm, *Mythimna separata* and was termed growth-blocking peptide (GBP) due to the paralysis that resulted from injection of larval hemolymph into another insect from the same species (Skinner et al., 1991). Following this initial discovery of GBP, another peptide, termed plasmotocyte spreading peptide (PSP) was isolated from *Pseudoplusia includens* (Skinner et al., 1991). These initial discoveries of these bioactive peptides have sparked interest in their structure and biological functions in other species. As such, the 25 amino acid long peptide, termed SRP for its role in regulating the immune response of insects., was identified in the hemolymph of *Spodoptera litura* in 2012 (Yamaguchi et al., 2012). Similarly, to other such peptides, SRPs are expressed as pre-pro-peptides and are functionally inactive in this form (Tsuzuki et al., 2012; Nakatogawa et al., 2009). Liberation of the active peptide from its pre-pro form is realized through action of extracellular serine proteases or intracellular enzymes (Hayakawa et al., 1995a; Wang et al., 1999; Nakatogawa et al., 2009).

In this chapter, we describe structural features of two SRPs, SRP-1 and SRP-2. We detail structural changes endowed by mutations at an embedded residue position and offer a structural basis for the differences in SRP-1/-2 receptor recognition and thus, biological functions.

1.1.2. Structure and biological function

As mentioned above, functionally active SRPs represent the C-terminal domain of much larger precursors with a pre-pro-peptide structure. Evidence suggests that the pre-region acts as a signal for secretion and, after its removal, the mature proteins either become extracellular precursors or are temporarily stored in secretory vesicles (Nakatogawa et al., 2009). ProSRPs are typically 40-130 residues long and poorly conserved in their N-terminal region (Matsumoto et al., 2012; Hayakawa et al., 1995; Volkman et al., 1999; Wang et al., 1999). Liberation of the C-terminal active peptide is accomplished through specific proteolytic cleavage by extracellular proteases (Hayakawa et al., 1995b; Wang et al., 1999). Evidence suggests that mature SRPs are involved in plasmatocyte spreading, hemocyte proliferation, insect paralysis, and wound healing by binding to receptors on the cell surface (Beschin et al., 2012; Dembic et al., 2015).

The SRP core region, corresponding to residues C8 – P21 of *Manduca sexta* SRP1 (Schrag et al., 2019), has a well-defined and consistent structure. Contrastingly, the N-terminal region of SRPs is largely unstructured (Aizawa et al., 1999; Miura et al., 2002; Volkman et al., 1999; Umetsu et al., 2009; Yu et al., 1999) and seems to be involved in proteolytic activation and specific binding to receptors (Umetsu et al., 2009; Strand et al., 2000; Matsumoto et al., 2012; Clark et al., 1997). The C-terminal region of SRPs on the other hand, has the greatest variety of amino acid composition, structure, and regulatory mechanisms observed when compared to the N- terminal region (Aizawa et al., 1999; 2001; Clark et al., 2001; Miura et al., 2002; Zhang et al., 2011).

The NMR solution structures of synthetic SRP-1 and SRP-2 *Manduca sexta* were determined in our laboratory using 2D ^{1}H-^{1}H NMR spectroscopy and Nuclear Overhauser

Effect (NOE) derived distance constraints. These studies showed that mature SRP-2 is composed of two short β-strands at R12−R15 and I18−V20, one type-I' β-turn at R15−I18, and a half turn at C8−S10 (Schrag et al., 2017). The structure of mature SRP-2 is stabilized by a covalent disulfide bond between C8 and C19. Similarly, SRP-1 was found to display an ordered structure consisting of two short β-strands at Y12−R15 and F18−F20, one type-II β-turn at R15−F18 in its core and is stabilized by a covalent disulfide bond between C8 and C19 (Schrag et al., 2017 and 2019).

Manduca sexta SRP-1 and SRP-2 sequences are 67.5% identical and 75% similar, and they also show a similar function of antimicrobial peptide expression (Schrag et al., 2017 and 2019). Structural comparison of the two peptides indicates that the most intriguing residue is located at position 12 (Y12 in SRP-1 and R12 in SRP-2). Previous NMR structural calculations show a large number of ^{1}H-^{1}H NOE contacts between the sidechains of residues 12, C8, P9 and C19 in both peptides as shown in Figure 1.1.

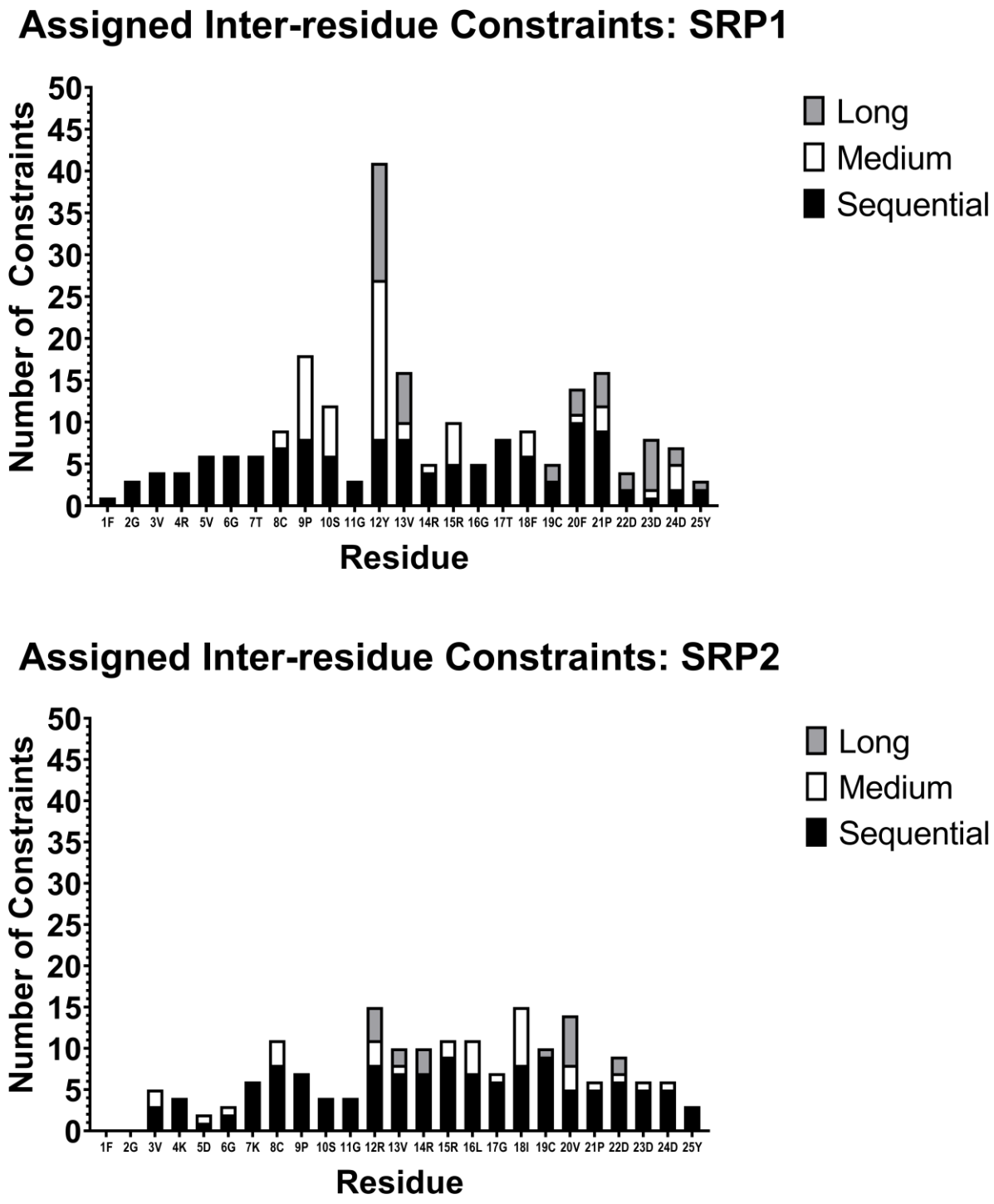

Figure 1. 1 NOE contacts per residue in SRP-1 and SRP-2. Sequential-range (i, j = i+1, black), medium-range (i, i+2 ≤ j ≤ i+4, white), and long-range (i, j ≥ i+5, grey) NOE contacts.

The high density of long-range NOE contacts for both peptides are akin to those observed earlier for residue Y11 in both plasmocyte spreading peptide of *Pseudopulsia includes* (PiPSP) (Volkman et al., 1999) and paralytic peptide of *Manduca sexta* (MsPP) (Yu et al., 1999). These studies suggested that residue Y11 plays an important role in the stabilization of PiPSP and MsPP structures (Clark et al., 2001). It was also observed that replacement of Y11 in PiPSP substantially reduced the biological activity in comparison to wild type (Clark et al., 2001). To better understand the role of residue Y12 and R12 in maintaining the structural stability of SRP-1 and SRP-2, we have conducted molecular dynamics studies of SRP-1 and -2 wild type and select mutants (Y/R12A, Y/R12E, R12K, Y12R and R12Y). The results presented here represent the first atomistic molecular dynamic analysis of SRP WT and variants in solution.

1.2. Materials and Methods

1.2.2. Explicit Solvent Simulation

The five lowest energy structures from the NMR ensemble (PDB entry 6EE9 for SRP-1 and 5W54 for SRP-2) consisting of 20 structures were selected for simulation. Mutations were made using the CHARMMGUI software PDB reader function (Jo et al., 2014). Single point mutations were introduced by replacing the amino acid sidechains while maintaining backbone coordinates. Residue number 12 of both peptides was mutated, resulting in the mutants Y12A, Y12E, Y12R for SRP-1 and R12E, R12A, R12Y, and R12K for SRP-2. Each of the five replicas for both SRP-1/-2 peptides was solvated in a cubic TIP3P explicit solvent water-box with an average volume of ~55 x 55 x 55$Å^3$ in CHARMM36 (Brooks et al., 1983 and 2009; Mark et al., 2001). Five 600-ns production simulations at standard temperature and pressure

were performed using NAMD, together yielding a total of 3.0μs effective sampling for SRP-1/-2 production simulations (Humphrey et al., 1996). Particle mesh Ewald was used for long-range electrostatic interactions and van der Waals interactions were smoothly switched off from 12 to 13Å (Darden et al., 1993). Hydrogen mass was increased to 3 a.m.u. through bound heavy atom mass repartition using an in-house script (Hopkins et al., 2015). The system was charge neutralized with K^+ and Cl^- atoms depending on the model used. Each of the solvated SRP-1/-2 structures was then energy minimized and equilibrated for 100 ps in the CHARMM36 force field (Huang et al., 2013). A dynamic time step of 4.0-fs was used, and SHAKE was applied to constrain the lengths of all bonds involving hydrogen atoms.

1.2.3. Structural and Clustering analysis

All structural and clustering analyses were performed using GROMACS and in-house scripts. Validation of successful agreement between the NMR and MD simulation data were performed by back-calculation of the weighted distance average observed for all WT SRP-1/-2 replicas during the simulation. The pair-wise upper-bound distances imposed for medium- and long-range constraints during solution structure determination were then compared with the weighted distance average values. Molecular visualization was performed using VMD (Humphrey et al., 1996). Root-mean-square-fluctuation (RMSF) calculations were performed by selecting Cα atom using the GROMACS gmx RMSF utility. The average RMSF values for all five selected NMR ensemble structures were calculated and plotted for the Wild Type (WT) and mutant peptides. Secondary structural characteristics analyses of SRP-1 and SRP-2 were accomplished through classification of each unique snap-shots' backbone dihedrals and hydrogen-bond contacts per residue. These contacts were then compared to assignments

consistent with the DSSP2.2.1 definitions to assess helical and β-strand formation for every residue in each peptide for the full 3004 snapshots for each SRP-1/-2 variant. The helical and β-strand propensities were then calculated on a per residue basis for the full 3004 snapshots for each unique SRP-1 and SRP-2 variant. Average end-to-end distances were measured by following the pair-wise distance between the N-terminal amine N atom and C-terminal carboxyl C atom for all 3004 snapshots. Pair-wise direct and pseudo-salt-bridge contact propensities were measured with the salt-bridge plug-in (Humphrey et al., 1996) for VMD with a heavy-atom cut-off distance of 4.25Å for both arginine and lysine residue types.

1.3. Results and Discussion

1.3.2. WT SRP-1 and SRP-2 simulations show agreement with NMR structure calculations

To appropriately assess the impact of *in silico* mutations of the embedded residue at position 12 for SRP-1 and SRP-2, validation of successful agreement between the NMR and MD simulation data was accomplished. This was done via back-calculation of the weighted distance average observed for all replicas of simulation for SRP-1/-2. The pair-wise upper-bound distances imposed for medium- and long-range NOE constraints during NMR solution structure determination were then compared with the weighted distance average values (Tables 1.1 and 1.2). SRP-1 demonstrates strong agreement with NMR structure distance constraints in the core region (residues C8-P21) but shows consistent NOE constraint violation for residues D22-Y25 (Table 1.1). Contrastingly, SRP-2 shows several NOE violations in the core region (C8-P21) but shows reasonable agreement with NMR structure distance constraints for residues D22-Y25 (Table 1.2).). Overall, the small values of overall distance violation suggest reasonable agreement between the NMR and MD simulation data for of WT SRP-1 and SRP-2.

Table 1. 1 Summary of NOE Violations for SRP1.

Medium-range	NOE constraint Upper-bound distance (Å)	Simulation Weighted distance (Å)	NOE Violation(Å)
HB1CYS8-HB2TYR12	6.0	2.8	-
HB2CYS8-HB2TYR12	4.5	3.1	-
HASER10-HNTYR12	6.0	3.7	-
HNARG15-HNPHE18	6.0	3.6	-
HAPRO21-HNASP24	4.5	6.7	2.2
HB2PRO21-HNASP24	6.0	5.9	-
HG1PRO21-HNASP24	6.0	7.0	1.0
HG2PRO21-HNASP24	6.0	7.0	1.0
HNASP23-HNTYR25	6.0	5.9	-
Long-range			
HB1CYS8-HB1CYS19	3.5	3.6	0.1
HB1TYR12-HB2CYS19	6.0	3.8	-
HATYR12-HAPRO21	6.0	2.7	-
HATYR12-HNASP24	4.5	7.0	2.5
HB1TYR12-HB1ASP23	6.0	7.0	1.0
HNVAL13-HB1ASP23	6.0	7.0	1.0
HNVAL13-HNASP24	6.0	7.0	1.0
HBVAL13-HB1ASP23	6.0	5.3	-
HG1VAL13-HNPHE20	6.0	4.4	-
HG1VAL13-HB1ASP23	6.0	5.6	-
HG2VAL13-HNPHE20	6.0	5.1	-
HG2VAL13-HB1ASP23	6.0	6.9	0.9

Table 1. 2 Summary of NOE Violations for SRP2*.

Medium-range	NOE constraint Upper-bound distance (Å)	Simulation Weighted distance (Å)	NOE Violation(Å)
HG1VAL3-HNASP5	4.5	4.1	-
HG2VAL3-HNASP5	4.5	4.1	-
HG1VAL3-HNGLY6	4.5	5.9	1.4
HG2VAL3-HNGLY6	4.5	5.9	1.4
HG1VAL13-HNARG15	5.0	5.2	0.2
HNARG15-HNGLY17	4.5	4.4	-
HNLEU16-HNILE18	6.0	4.8	-
HALEU16-HNILE18	4.7	4.9	0.2
HB1LEU16-HNILE18	6.0	7.0	1.0
HNILE18-HG2VAL20	6.0	7.0	1.0
HBPRO21-HNASP23	4.5	4.9	0.4
HAASP22-HNASP24	6.0	4.8	-
Long-range			
HG1VAL13-HNCYS19	6.0	7.0	1.0
HG2VAL13-HNCYS19	6.0	7.0	1.0
HG1ARG12-HNVAL20	6.0	6.0	-
HG1ARG12-HNASP22	6.0	5.1	-
HG2ARG12-HNASP22	6.0	5.0	-
HD1ARG12-HNVAL20	6.0	6.0	-
HNVAL13-HNVAL20	4.5	4.2	-
HAARG14-HNVAL20	4.5	4.0	-
HBARG15-HNVAL20	6.0	6.1	0.1
HGARG14-HNVAL20	6.0	5.8	-

*Adapted from Schrag, L. G (2020).

1.3.3. Substitutions at the embedded position reveal differences in SRP-1 and SRP-2 internal motions

To assess the impact of mutations at the embedded position (residue-12) upon residue mobility, root-mean-square-fluctuation (RMSF) calculations were performed. Figure 1.2 shows average per residue RMSF of wild-type and mutants of SRP-1and SRP-2. The overall peptide core region's (residues 8-22) RMSF values for SRP-1 and its mutants fluctuate between 0.2-0.5 nm while RMSF values for SRP-2 and its mutants RMSF values stay within the 0.3-0.8 nm range suggesting that SRP-1 has an overall more rigid structure than SRP-2. All mutations

introduced at the embedded position (residue 12) in SRP-1 show considerable increase in overall flexibility of the peptide in comparison to wild type as illustrated by the higher RMSF values observed for residues G6-F18. In contrast, SRP-2 mutants show relatively similar RMSF values to the WT peptide across all residues, suggesting that SRP-2 mutants have similar overall rigidity to SRP-2 WT. These results infer that SRP-1 is inherently more rigid within the core and that substitutions at the embedded position have a large effect on the peptide's internal motion. In contrast, SRP-2 WT appears more intrinsically dynamic within the core region as embedded residue substitution displays little effect upon the molecule's overall plasticity. This discrepancy observed between SRP-1 and SRP-2's internal motions represent a new insight in structural differences between these two cytokines as NMR analysis showed little structural discrepancy between SRP-1 and SRP-2 (Schrag et al., 2017 and 2019).

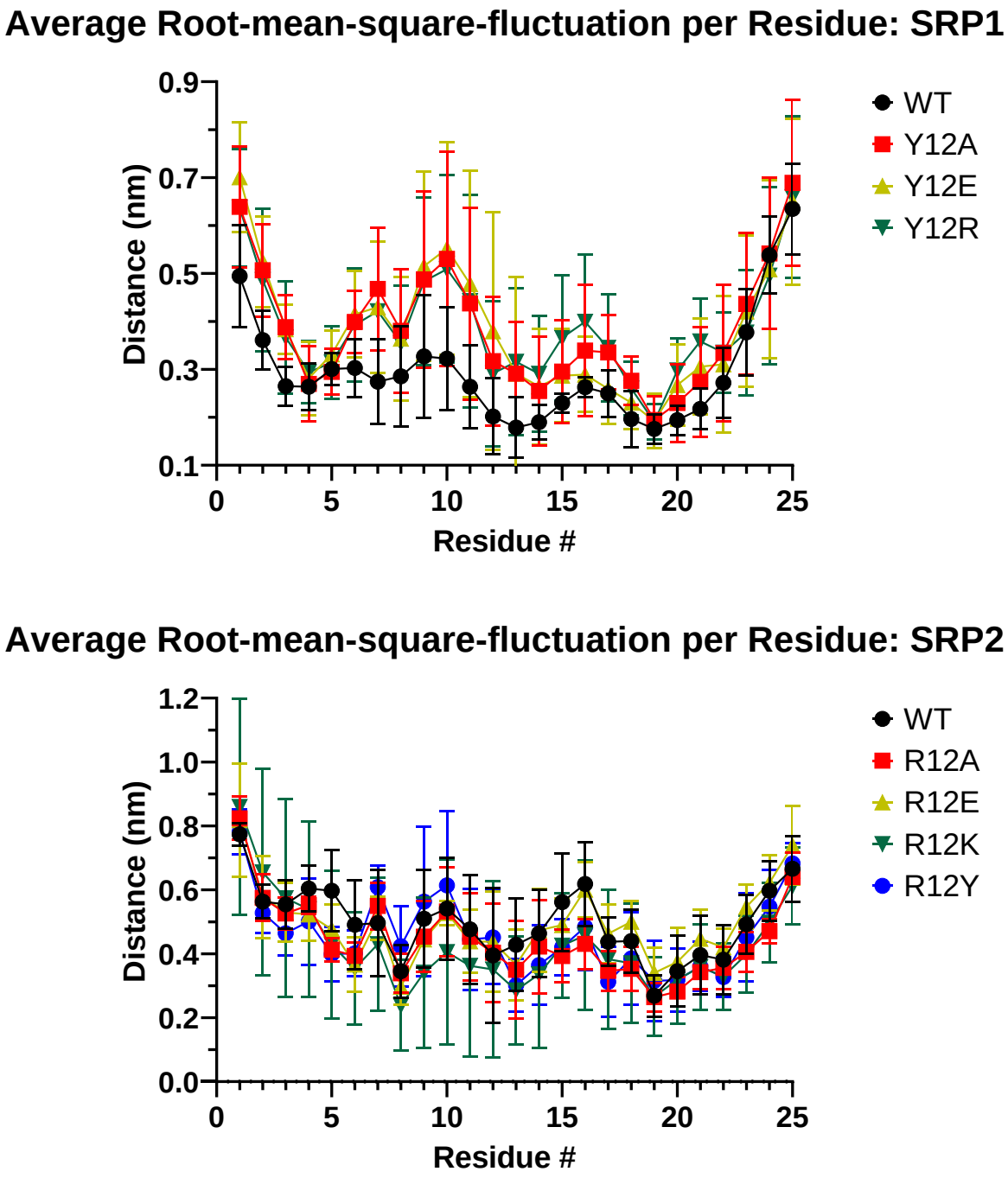

Figure 1. 2. Average per residue root mean square fluctuation of SRP-1 and SRP-2 wild type/mutants. SRP-2 figure is adapted from Schrag, G. L., 2020.

1.3.4. Secondary Structural propensity analyses uncovers the existence of previously unassigned N-terminal structural features in SRP2

RMSF calculations (Figure 1.2) suggested an increased motility of core region residues of SRP-1 mutants in comparison to WT, while SRP-2 mutants display little deviation from WT. Because an increase in core region mobility does not necessarily imply change in secondary structure, β-strand formation propensities, as well as Helical propensities of SRP-1/-2 were calculated (Figure 1.3).

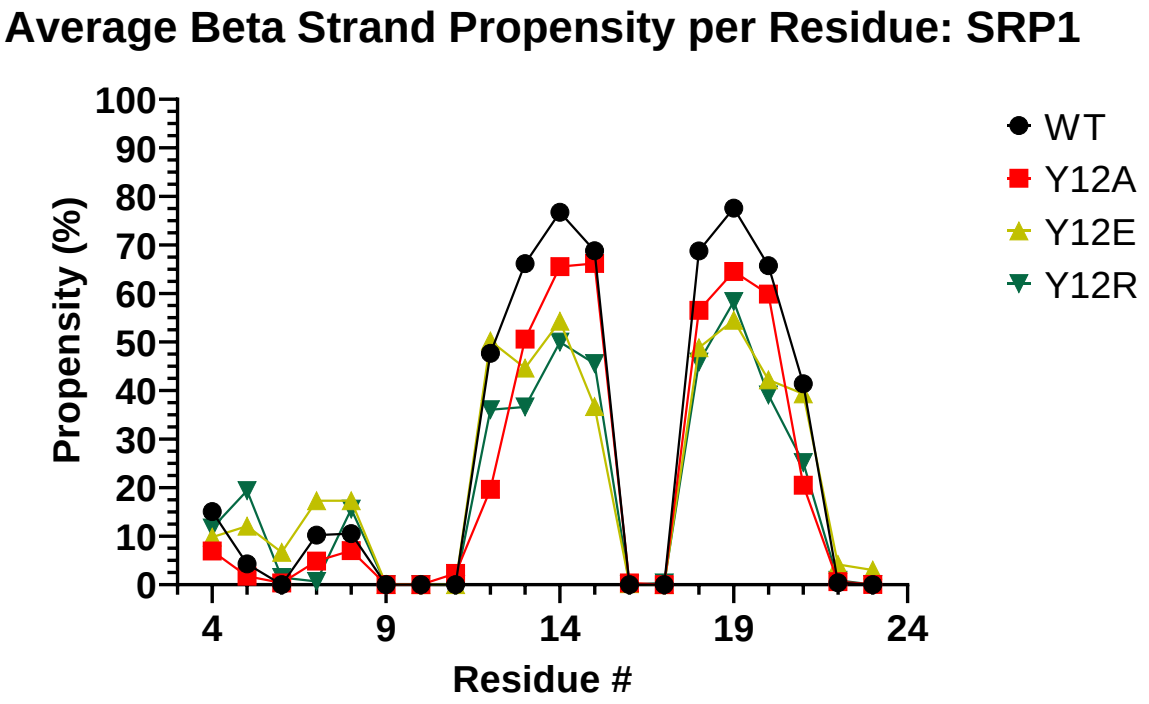

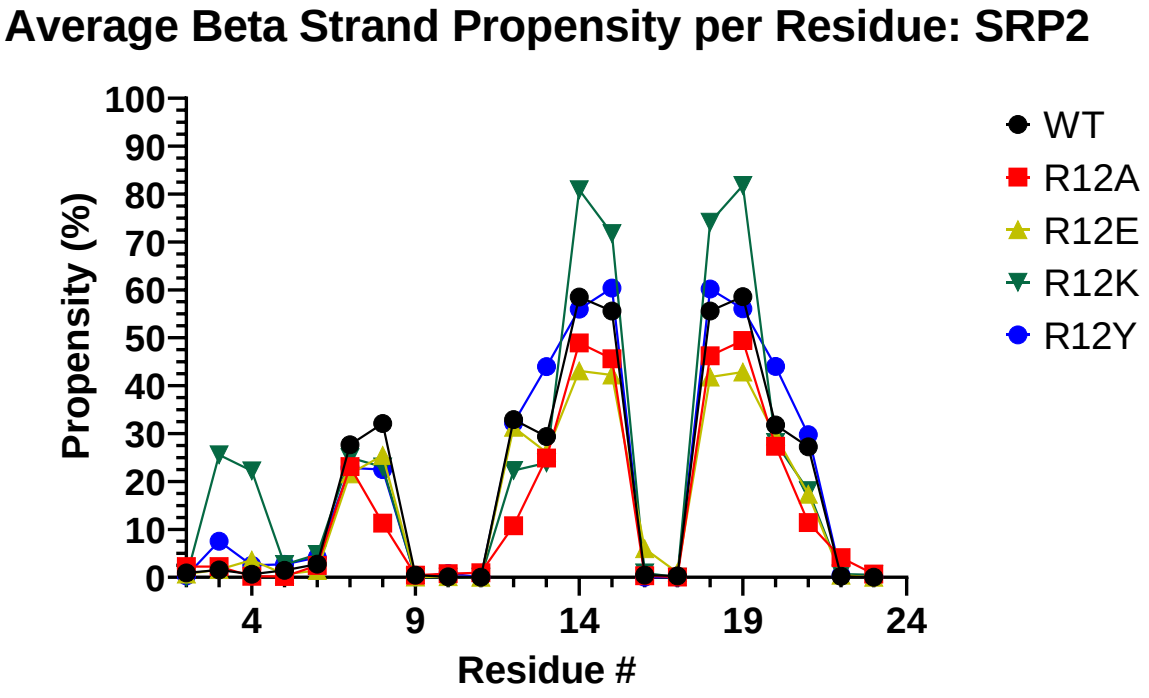

Figure 1. 3 Average beta strand propensity per residue for SRP-1/2 and mutants. SRP-2 figure is adapted from Schrag, G. L., 2020.

SRP-1 WT shows the highest propensity for β-strand formation for residues Y12-R15 and F18-P21 while all analyzed mutants show a lower β-strand formation propensity in comparison to WT. Despite the lower β-strand formation propensity, SRP-1 Y12A seems to retain WT structural features better than all other mutants studied. In accordance with the increase in overall flexibility for all SRP-1 mutants observed with RMSF calculations for residues Y12-R15 and F18-P21, the decrease in β-strand formation propensity suggests disruption of this secondary structural feature as a result of residue Y12 substitution. In contrast, SRP-2 WT shows a propensity for β-strand formation for residues R12-R15 and F18-P21 of about 60% (Figure 1.3). These observations are in agreement with NMR the chemical shift values indicating β-strands for residues R12-R15 and I18-V20 for SRP-2 and SRP-1. SRP-1 displayed a backbone only RMSD of 0.28 ± 0.08Å for residues 8-23, while SRP-2 displayed one of 0.87 ± 0.21Å for residues 8-21 (Schrag et al., 2017; 2019), suggesting that SRP-2's core region may be less rigid than SRP-1's. The lower β-strand formation propensity of SRP-2 suggests that the higher RMSD observed translates to a more flexible β-strand. In contrast with SRP-1, SRP-2 variant R12K shows a higher β-strand formation propensity than SRP-2 WT while the R12Y variant shows a similar propensity to WT. Conversely, SRP-2 R12A and R12E variants show lower β-strand formation propensities when compared to WT. These observations suggest that SRP-2 mutant R12Y retains SRP-2's native secondary structural characteristics within the core region. The discrepancy in the structural impacts of residue 12 substitutions present new insights into the role of this residue in core region stabilization for SRP-1 and SRP-2. These mutations seem to have a more drastic effect on SRP-1's overall flexibility and β-strand formation while the effects are more varied for SRP-2, suggesting that other factors may be at play in terms of core region stabilization for SRP-2.

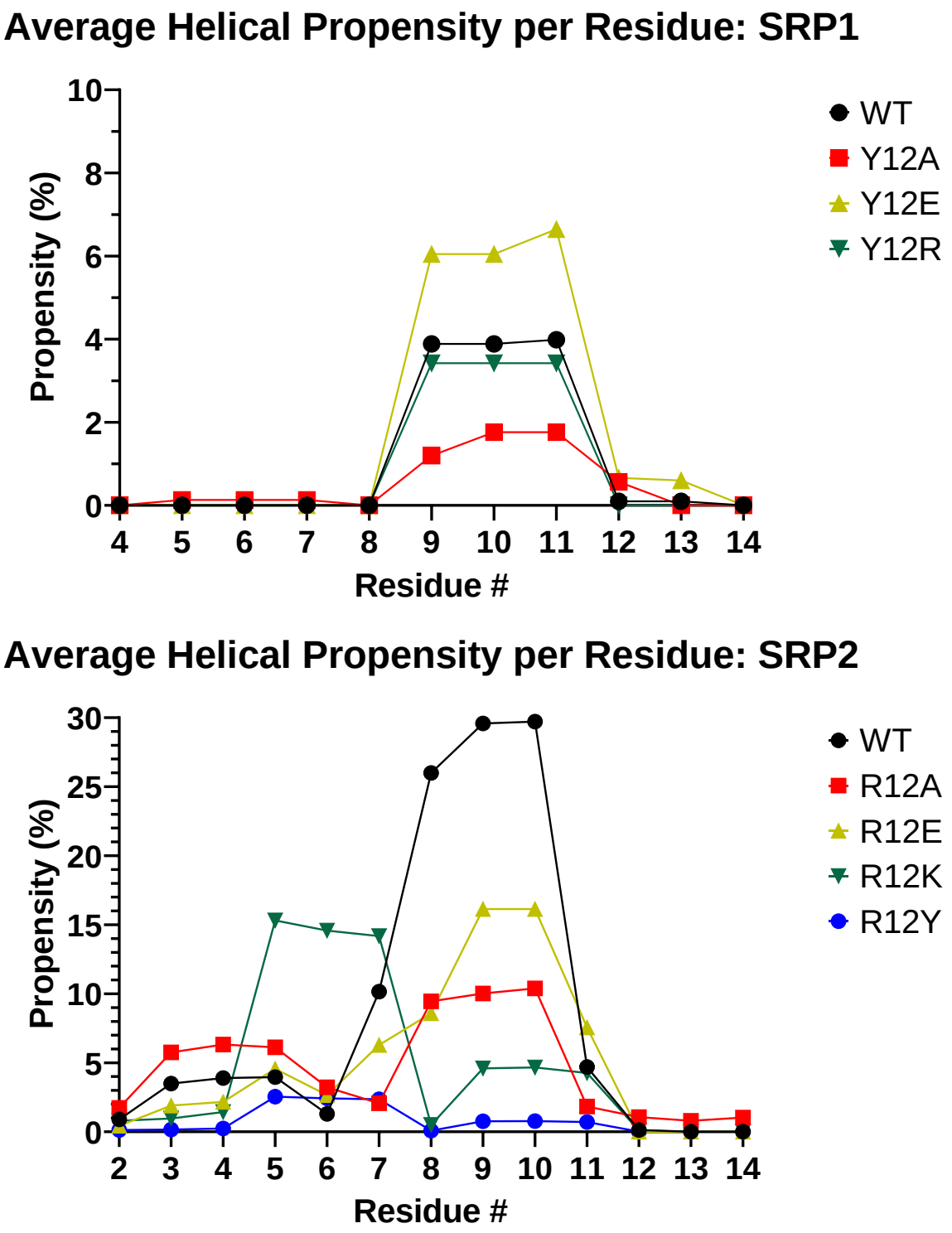

Figure 1. 4 Average helical strand propensity per residue for SRP-1/2 and mutants. SRP1 figure is adapted from Schrag, G. L., 2020.

Expanding the scope of the secondary structural analysis to include residue positions beyond the core region revealed the presence of previously uncategorized secondary structural features. Specifically, SRP-2 WT displays a short β-strand for residues positions K7 and C8 with a propensity of ~30%. This feature is not faithfully replicated by any SRP-2 variant analyzed, nor is it present in any SRP-1 variants. This suggests the existence of secondary structures further into N-terminus than previously categorized. Considering this observation in SRP-2, we posited that other secondary structural features, may have been overlooked from NMR due to their transient nature.

To address this, helical formation propensities were calculated for all SRP-1 and SRP-2 variants. As expected, SRP-1 WT shows a helical propensity of only ~4%, while the variant Y12A shows ~2%, Y12E ~6%, and Y12R ~4% for residues P9, S10, and G11 (Figure 1.4). These results suggest that helicity is not a major contributor in the structure of SRP-1. Contrastingly, SRP-2 WT shows a helical propensity of ~27.5% for residues C8, P9 and S10 (Figure 1.4). Similarly, to β-strand formation, no SRP-2 variant was able to replicate SRP-2 WT's helical propensity. These observations suggest that residue type at the embedded position has little impact upon the preferred N-terminal secondary structure of SRP-1, our observations suggest the opposite for SRP-2.

β-strand and helix formation propensities for SRP-1/-2 suggested that the embedded residue at position 12 plays a critical role in SRP-1's core region stability. Contrastingly, SRP-2's core region seems to be stabilized by the existence of a N-terminal helix in addition to the stabilizing effects of the embedded residue, as shown by the higher helical propensity for SRP-2's N-terminal region. These results offer an explanation as to why SRP-1 and SRP-2 mutants

show such divergent RMSF profiles and secondary structural characteristics: substitutions at the embedded position in SRP-1 show increased flexibility and disruption of the β-strand because SRP-1 lacks the additional stabilizing effect of a N-terminal helix, a feature present in SRP-2. In all, these results imply that the role of the embedded residue is more complicated than previously proposed and that perhaps the role of the embedded residue in SRPs also regulates the orientation of N-terminus, a region that has been shown to be critical in imparting mitogenic activity.

1.3.5. SRP-2 variants are more heterogenous than SRP-1 variants in clustering analysis

To gain insight into the potential differences in tertiary structural dynamics suggested by the RMSF and secondary structurally analyses, an initial analysis of ensemble heterogeneity for all SRP-1 and SRP-2 variants against their respective WT ensembles was completed. Results of SRP-1 variants using this approach reveal that the four most populated clusters show representations of 72.8% for WT simulations, 51.0% for Y12A, 49.9% for Y12E, and 50.6% for Y12R (Figure 1.5). It is evident and largely reflective of RMSF observations that SRP-1 WT is the least heterogeneous of the four variants. Moreover, SRP-1 WT is the only ensemble that retains secondary structure for the most populated states.

In contrast, SRP-2's four most populated clusters for each variant reveal representations of 47.4% for WT simulations, 29.7% for R12A, 30.7% for R12E, 61.3% for R12K, and 54.7% for R12Y (Figure 1.6). These observations are consistent with β-strand propensities of the core region. In addition, the presence of the transient N-terminal secondary feature is quite robustly represented in SRP-2 WT ensembles and is quite distinctively absent in variant clusters. This reinforces the notion that the role of the embedded residue on the stabilization of

the core region of SRP-1 and SRP-2 is quite distinct. In SRP-1 residue Y12 appears to promote overall steric restriction and core region stability, while in SRP-2, the R12 residue partially sacrifices maximal steric restriction in favor of greater secondary structure formation in the N-terminus. These differences in peptide structural dynamics and, more importantly, N-terminal orientation may offer a basis for SRP-1 and SRP-2's distinct functions and expression profiles.

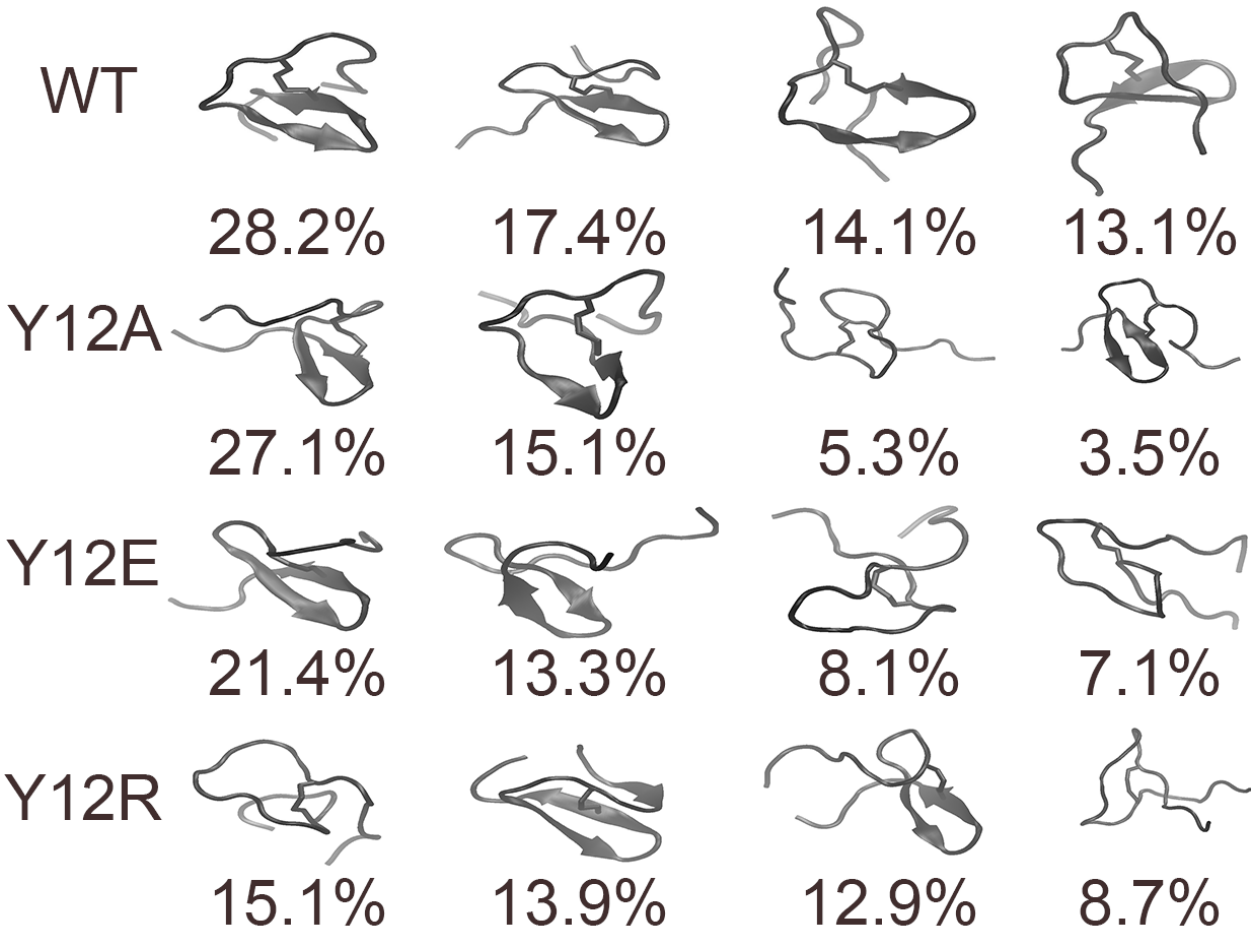

Figure 1. 5 Cluster Heterogeneity Analysis of Simulated SRP-1 and mutants.

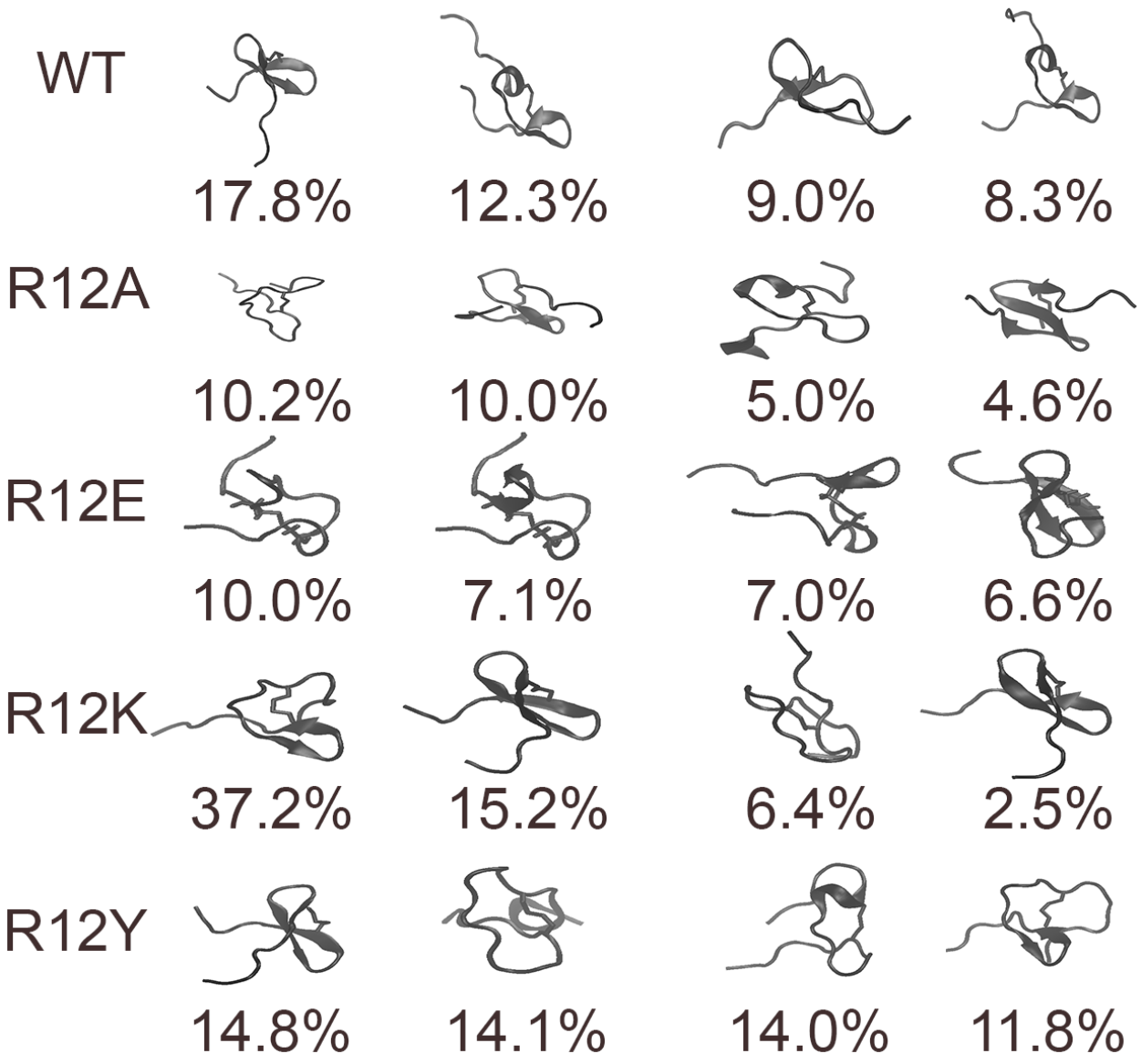

Figure 1. 6 Cluster Heterogeneity Analysis of Simulated SRP-2 and mutants. Adapted from Schrag, G. L., 2020.

1.3.6. SRP-1 and SRP-2 display opposite End-to-End distance, and Salt-Bridge formation profiles

The general lack of secondary structure for residues T7 through G11 in SRP-1, and the prevalence of such structures in SRP-2 suggested differences in the N-terminal orientation relative to the C-terminus between the two peptides. Assessment of SRP-1 and SRP-2 end-to-

end distances (Figure 1.7) reveals that SRP-1 WT is the most compact (11.8 ± 6.8 Å) of all variants analyzed, while SRP-2 WT (Figure 1.7) is the most extended (21.0 ± 7.3 Å). Interestingly, no SRP-1 or SRP-2 variant was able to faithfully replicate WT profiles. The more compact nature of SRP-1 WT, and the failure of the variants to replicate WT's profile suggest that the more extended structure of SRP-1 variants may stem from a disruption of secondary structural features, mainly the β-strand, resulting in a higher RMSF value. In the case of SRP-2 however, the more extended structure of WT in comparison to mutants suggest that substitutions at the embedded position may disrupt critical interactions in SRP-2 WT responsible for N-terminal orientation.

In all, when compared against their respective variants, all SRP-1 variants display increased end-to-end distances, while the converse is true for SRP-2. The numerous transient N- to C-terminal contacts for SRP-2 WT may provide insight onto critical termini orientations and their subsequent role in receptor selectivity by SRP-1/-2.

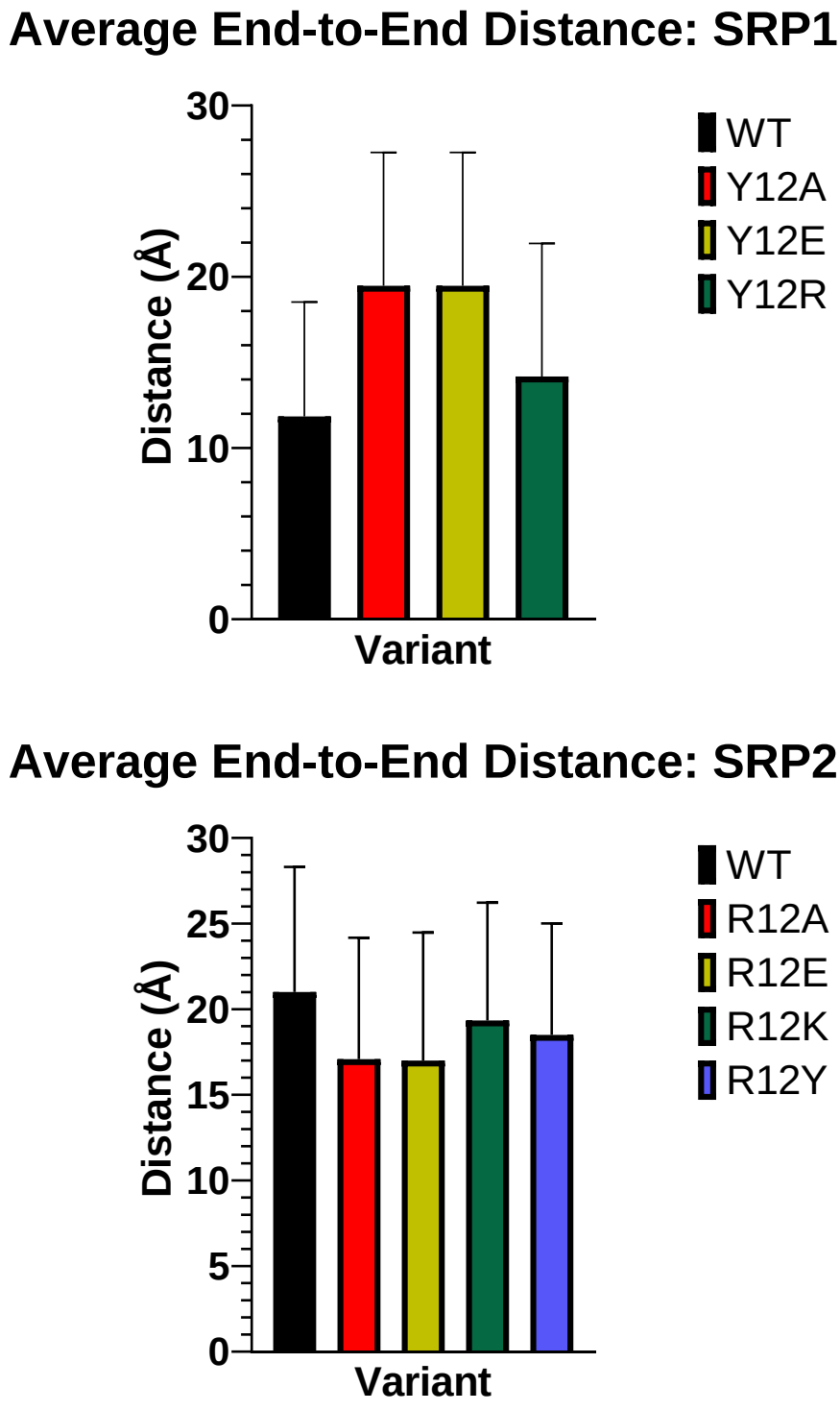

Figure 1. 7 Average End-to-End Distance: SRP-1 and SRP-2. SRP-2 figure adapted from Schrag, G. L., 2020.

Subsequent analysis of the end-to-end trajectories reveals that SRP-2 makes numerous transient direct N- to C-terminus salt-bridge contacts in contrast to SRP-1's sparse number of interactions. An assay of both direct- and pseudo-contacts between salt-bridges was thus undertaken. Results show that SRP-1 WT makes a prominent ARG4-ASP22 contact which is best reproduced by mutant SRP-1 Y12A (Figure 1.8). In contrast, only SRP-2 WT was observed to make LYS7-ASP22, and LYS7-ASP24 contacts while all other mutants fail to replicate WT's salt-bridge propensities (Figure 1.8). These results indicate that the amino acid Arginine at position 12 is the only residue type that facilitates this salt-bridge contact in SRP-2. The lack of a LYS7-ASP22/24 salt-bridge contact in SRP-1 may explain the observed differences in secondary structure propensities observed for all SRP-1 variants (Figure 1.8). These observations imply that the presence of these secondary structural differences and distinct N-terminal orientations have significant implications upon receptor selection for SRP-1/-2, and thus their biological function.

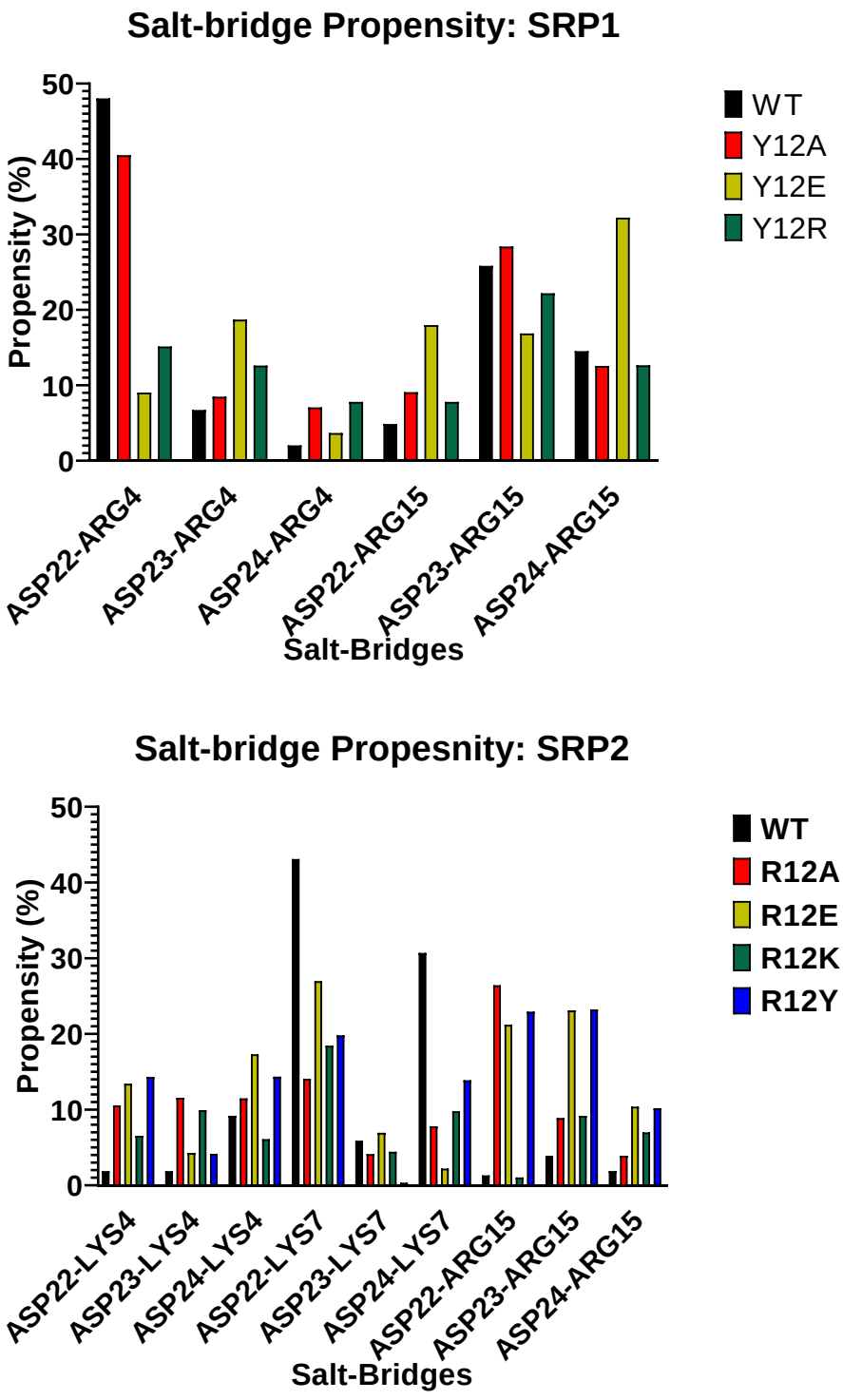

Figure 1. 8 Salt-bridge Formation Propensity : SRP-1 and SRP-2. SRP-2 figure adapted from Schrag, G. L., 2020.

1.4. Conclusions

NOE back-calculations demonstrate that SRP-1/-2 WT's NMR features are faithfully replicated *in silico*. Subsequent root-mean-square-fluctuation calculations, secondary structural and clustering analyses reveal that SRP-1 WT's core region is the most structurally rigid of all SRP-1 variants analyzed, while SRP-2 WT is flexible within the core region. SRP-1 lacks propensities for both helical and β-strand formation for residues T7 through G11, while SRP-2 demonstrates a greater propensity for both helical and β-strand formation for these residues. These observations suggest that other factors, namely N- and C-terminal salt-bridge contacts, may be involved in the stabilization of SRP-2's core region, and that these two peptides have markedly different N- to C-terminal orientation features. End-to-end analysis shows that SRP-1 wild type is the most compact of all variants analyzed, while SRP-2 wild type is the most extended. These results are consistent with RMSF calculations showing more rigid SRP-1 and more flexible SRP-2 wild type core regions. Salt-bridge analysis revealed that SRP-1 WT forms a favorable interaction between R4 and D22 while SRP-2 WT forms salt-bridges between K7, D22 and D24. These differences imply that these secondary structures and/or N-terminal orientations observed may have significant implications upon selection of target receptor(s) for SRP-2 and SRP-1.

1.5. References

Aizawa, T., Fujitani, N., Hayakawa, Y., Ohnishi, A., Ohkubo, T., Kumaki, Y., Kawano, K., Hikichi, K., & Nitta, K. (1999). Solution structure of an insect growth factor, growth-blocking peptide. *Journal of Biological Chemistry*, *274*(4), 1887–1890.

Aizawa, T., Hayakawa, Y., Ohnishi, A., Fujitani, N., Clark, K. D., Strand, M. R., Miura, K., Koganesawa, N., Kumaki, Y., Demura, M., Nitta, K., & Kawano, K. (2001). Structure and activity of the insect cytokine growth-blocking peptide: Essential regions for mitogenic and hemocyte-stimulating activities are separate. *Journal of Biological Chemistry*, *276*(34), 31813–31818.

Beschin, A., & Müller, W. E. G. (2012). *Invertebrate Cytokines and the Phylogeny of Immunity : Facts and Paradoxes*. Springer Berlin Heidelberg.

Brooks, B. R., Brooks III, C. L., Mackerell Jr., A. D., Nilsson, L., Petrella, R. J., Roux, B., Won, Y., Archontis, G., Bartels, C., Boresch, S., (2009). CHARMM: the biomolecular simulation program. Journal of computational chemistry, 30 (10), 1545-1614.

Brooks, B. R., Bruccoleri, R. E., Olafson, B. D., States, D. J., Swaminathan, S. A., Karplus, M. (1983) CHARMM: a program for macromolecular energy, minimization, and dynamics calculations. Journal of computational chemistry, 4 (2), 187-217

Clark, K. D., Pech, L. L., & Strand, M. R. (1997). Isolation and identification of a

plasmatocyte-spreading peptide from the hemolymph of the lepidopteran insect Pseudoplusia includens. *Journal of Biological Chemistry*, *272*(37), 23440–23447.

Clark, K. D., Volkman, B. F., Thoetkiattikul, H., Hayakawa, Y., & Strand, M. R. (2001). N-terminal Residues of Plasmatocyte-spreading Peptide Possess Specific Determinants Required for Biological Activity. *Journal of Biological Chemistry*, *276*(40), 37431–37435.

Clark, K. D., Volkman, B. F., Thoetkiattikul, H., King, D., Hayakawall, Y., & Strand, M. R. (2001). Alanine-scanning Mutagenesis of Plasmatocyte Spreading Peptide Identifies Critical Residues for Biological Activity. *Journal of Biological Chemistry*, *276*(21), 18491–18496.

Darden, T., York, D., Pedersen, L. (1993) Particle mesh Ewald: An N· log (N) method for Ewald sums in large systems. *The Journal of chemical physics*, 98 (12), 10089-10092.

Dembic, Z. (2015). The cytokines of the immune system: The role of cytokines in disease related to immune response. Academic Press.

Duressa, T. F., Boonen, K., Hayakawa, Y., & Huybrechts, R. (2015). Identification and functional characterization of a novel locust peptide belonging to the family of insect growth blocking peptides. *Peptides*, *74*, 23–32.

Hayakawa, Y. (1995a). Growth-blocking peptide: an insect biogenic peptide that prevents the onset of metamorphosis. In *Journal of Insect Physiology* (Vol. 41, Issue 1, pp. 1–6). Pergamon.

Hayakawa, Y., Ohnishi, A., Yamanaka, A., Izumi, S., & Tomino, S. (1995b). Molecular cloning and characterization of cDNA for insect biogenic peptide, growth-blocking peptide. *FEBS Letters, 376*(3), 185–189.

Hopkins, C. W., Le Grand, S., Walker, R. C., Roitberg, A. E., Long-Time-Step Molecular Dynamics through Hydrogen Mass Repartitioning. Journal of Chemical Theory and Computation **2015** 11 (4), 1864-1874.

Huang, J., MacKerell, A. D., Jr., CHARMM36 all-atom additive protein force field: validation based on comparison to NMR data. *Journal of computational chemistry* **2013**, 34 (25), 2135-2145.

Humphrey, W., Dalke, A., & Schulten, K. (1996). VMD: visual molecular dynamics. Journal of molecular graphics, 14(1), 33-38.

Jo, S., cheng, X., Islam, Shahidul., Huang, L., Huan, R., Zhu, A., Lee, H. S., Qi, Y., Han, W., Vanommeslaeghe, A., Roux, B., I, W. (2014). CHARMM-GUI PDB Manipulator for Advanced Modeling and Simulations of Proteins Containing Non-standard Residues. *Adv. Protein Chem. Struct. Biol.* 96, 235-265.

Matsumoto, H., Tsuzuki, S., Date-Ito, A., Ohnishi, A., & Hayakawa, Y. (2012). Characteristics common to a cytokine family spanning five orders of insects. *Insect Biochemistry and Molecular Biology*, *42*(6), 446–454.

Mark, P., Nilsson, L. (2001). Structure and Dynamics of the TIP3P, SPC, and SPC/E Water Models at 298 K. The Journal of Physical Chemistry A, 105 (43), 9954-9960.

Miura, K., Kamimura, M., Aizawa, T., Kiuchi, M., Hayakawa, Y., Mizuguchi, M., & Kawano, K. (2002). Solution structure of paralytic peptide of silkworm, Bombyx mori. *Peptides*, *23*(12), 2111–2116.

Nakatogawa, S. ichi, Oda, Y., Kamiya, M., Kamijima, T., Aizawa, T., Clark, K. D., Demura, M., Kawano, K., Strand, M. R., & Hayakawa, Y. (2009). A Novel Peptide Mediates Aggregation and Migration of Hemocytes from an Insect. *Current Biology*, *19*(9), 779–785.

Schrag, L. G, Cao, X., I. Herrera, A., Wang, Y., Jiang, H., & Prakash, O. (2017). Solution Structure and Expression Profile of an Insect Cytokine: *Manduca sexta* Stress Response Peptide-2. *Protein and Peptide Letters*, *24*(1), 3–11.

Schrag, L. G. (2020). *Biophysical studies of selected intrinsically disordered proteins: insect stress-response peptides and cancer-linked variants of human p53 transactivation domain* [AN ABSTRACT OF A DISSERTATION].

Schrag, L. G., Cao, X., Dembele, H., Liu, X., Al Souhail, Q., Robert Kanost, M., Chen, J., Jiang, H., & Prakash, O. (2019). Expression and Characterization of <i>Manduca sexta</i> Stress Responsive Peptide-1; An Inducer of Antimicrobial Peptide Synthesis. *Biochemistry and Molecular Biology*, *4*(3), 42.

Skinner, W. S., Dennis, P. A., Li, J. P., Summerfelt, R. M., Carney, R. L., & Quistad, G. B. (1991). Isolation and identification of paralytic peptides from hemolymph of the lepidopteran insects Manduca sexta, Spodoptera exigua, and Heliothis virescens. *Journal of Biological Chemistry*, *266*(20), 12873–12877.

Strand, M. R., Hayakawa, Y., & Clark, K. D. (2000). Plasmatocyte spreading peptide (PSP1) and growth blocking peptide (GBP) are multifunctional homologs. *Journal of Insect Physiology*, *46*(5), 817–824.

Tsuzuki, S., Ochiai, M., Matsumoto, H., Kurata, S., Ohnishi, A., & Hayakawa, Y. (2012). Drosophila growth-blocking peptide-like factor mediates acute immune reactions during infectious and non-infectious stress. Scientific reports, 2, 210.

Umetsu, Y., Aizawa, T., Muto, K., Yamamoto, H., Kamiya, M., Kumaki, Y., Mizugichi, M., Demura, M., Hayakawa, Y., & Kawano, K. (2009). C-terminal elongation of growth-blocking peptide enhances its biological activity and micelle binding affinity. *Journal of Biological Chemistry*, *284*(43), 29625–29634.

Volkman, B. F., Anderson, M. E., Clark, K. D., Hayakawa, Y., Strand, M. R., & Markley, J. L. (1999). Structure of the insect cytokine peptide plasmatocyte-spreading peptide 1 from Pseudoplusia includens. Journal of Biological Chemistry, 274(8), 4493-4496.

Wang, Y., Jiang, H., & Kanost, M. R. (1999). Biological activity of Manduca sexta paralytic and plasmatocyte spreading peptide and primary structure of its hemolymph precursor. *Insect Biochemistry and Molecular Biology*, *29*(12), 1075–1086.

Yamaguchi, K., Matsumoto, H., Ochiai, M., Tsuzuki, S., & Hayakawa, Y. (2012). Enhanced expression of stress-responsive cytokine-like gene retards insect larval growth. *Insect Biochemistry and Molecular Biology*, *42*(3), 183–192.

Yu, X.-Q., Prakash, O., & Kanost, M. R. (2010). Structure of a paralytic peptide from an insect, Manduca sexta. *The Journal of Peptide Research*, *54*(3), 256–261.

Zhang, S., Gunaratna, R. T., Zhang, X., Najar, F., Wang, Y., Roe, B., & Jiang, H. (2011) Pyrosequencing-based expression profiling and identification of differentially regulated genes from Manduca sexta, a lepidopteran model insect. *Insect biochemistry and molecular biology*, 41(9), 733-746.

2. NMR Solution Structure of Ecdysis Triggering Hormone Peptide from the African Malaria Mosquito *Anopheles gambiae*

2.1. Introduction

Numerous mosquitoes species are vectors of pathogens that often cause devastating infectious diseases, such as malaria, dengue, yellow fever, and Zika fever. Evidently, every year, more than 1 million deaths and up to 700 million cases of infections by mosquito-borne vector diseases are reported (Campbell-Lendrum et al., 2015). As a remedy for the devastating toll caused by these vectors, chemical insecticides have been a popular and highly efficient method for the disruption of the pathogen transmission cycle, leading to the suppression of the vector population. Though the widely available insecticides are effective against the vectors, the evolution of insecticide resistance has hampered their efficacy and causes a significant need for the development of new insecticidal methods. In particular, insecticides generally represent the most acutely toxic class of pesticides as they can be toxic to a multitude of other organisms including birds, mammals, and other beneficial insect populations (Aktar et al., 2009). These new regulations cause significant need for the discovery of new insecticide targets that would allow for lower toxicity and specificity towards mammals and other insect populations.

Ecdysis is a process during which insects shed their old cuticle for size growth during development and involves complex neuropeptidergic signals (Kim et al., 2006). The ecdysis sequence is usually divided into three phases: pre-ecdysis, ecdysis, and post-ecdysis. The pre-

ecdysis phases involve securing of the insect, and movement that leads to the disruption of muscle connections to the old cuticle (Truman, 2005). During the ecdysis phase, most insects display motor patterns that often involve rhythmic peristaltic contractions that move anteriorly along the body (Weeks et al., 1984; Zitnan et al., 1996). Post-ecdysis is characterized by the expansion and hardening of the new cuticle, a process that can aid in the rupturing of the old cuticle. This expansion often involves changes in cardiac activity and the swallowing of air or water to expand the body cavity (Truman, 2005). The initial signal for this sequence of behavioral events is the endocrine peptide, Ecdysis Triggering Hormone (ETH).

In this chapter, we describe the structure and function of ETH from various insects. By summarizing related paper, we provide an overview of the Ecdysis process and detail ways in which this process could be hacked to develop novel insecticidal compounds against the African malaria mosquito, *Anopheles gambiae.*

2.1.1. Discovery

The first indication of hormonal control of ecdysis emerged from studies on the giant silk moths, *Hyalophor cecropia* and *Antheraea pernyi*. Brain excision and implantation experiments between species showed the brain controls the timing and coordination of the sequential behavioral events leading to molting (Truman et al., 1970). While complete removal of the brain did not block the insects' ability to shed their cuticle, the coordinated sequence and timing of the events turned random (Truman, 1971). Restoration of the timing and coordination of the behavioral events later indicated that a hormonal component must be involved, the search for which yielded isolation and sequencing of the Eclosion Hormone (EH) from

Manduca sexta (Kataoka et al., 1987; Marti et al., 1987). Further characterization showed that *Manduca sexta* EH was a 62 amino acid peptide constrained by three disulphide bridges (Truman, 1971). While it is clear that EH is widely present within the Insecta, no evidence suggests its presence outside of this group.

Several years after the discovery and characterization of EH, a second peptide involved in ecdysis control was isolated in *Manduca sexta*. This hormone, termed the Ecdysis Triggering Hormone (ETH), is a 11 – 34 amino acid long amidated peptide secreted by the Inka cells and is widely distributed among insects (Zitnan et al., 2016). Isolation of the ETH gene from Manduca sexta showed cleavage of proETH into three peptides, MasETH, pre-ecdysis triggering hormone, and (MasPETH), both of which have a C-terminal PRXamide motif, and ETH-associated peptide (Truman, 2005). Expanding this search to other species, studies revealed that ETH in *Drosophila melanogaster* is also cleaved in two active peptides, DrmETH1 and DrmETH2 (Park et al., 1999). Similarly, two ETH peptides are encoded by the *Anopheles gambiae* precursor, of which, one is involved in pre-ecdysis while the other is involved later in the ecdysis sequence (Zitnan et al., 2003).

2.1.2. Biological function and structure

ETH peptides are essential and sufficient to evoke pre-ecdysis behavior, as shown in previous studies, ecdysis behavior can be effectively rescued by injecting KO mutants larvae with the peptide (Park et al., 2002). ETH was also found to work in the regulation of another crucial endocrine factor, juvenile hormone (JH) in mosquito involved in larval growth (Areiza et al., 2014; Nyati et al., 2013), as well as the control of reproduction in *Drosophila melanogaster*

(Meiselman et al., 2018). Previous studies have also detected ETH receptor (ETHR) transcripts in corpora allata, an organ responsible for the release of JH which has an important role in the regulation of development, courtship, and diapause, of *Bombix mori*, *Manduca sexta*, and *Drosophila melanogaster* (Shi et al., 2017 and 2019).

Most importantly, studies show that disruption of signaling by ETH leads to failure to inflate the new, developing, respiratory system and to perform the ecdysis behavioral sequence in *Drosophila melanogaster* and others (Park et al., 2002; Dai et al., 2008; Lenaerts et al., 2017; Shi et al., 2017), offering a potential target system for an insecticidal strategy. Looking at efforts towards structural characterization of ETH or ETHR, to date, no structure has been reported for these hormones or their receptors. ETH is part of a class of peptides termed PRXamide peptides as owing to the characteristic PRX-NH_2 C-terminal motif often crucial for receptor activation (Jiang et al., 2014). Mature *Anopheles gambiae* ETH is 17 amino acid long peptide of which the sequence is shown below in Figure 2.1. Figure 2.1 also shows a sequence alignment of ETH peptides from several species, highlighting heavily conserved residue positions across species, namely the two lysine residues at positions 9 and 12, as well as the characteristic PRXamide C-terminal motif.

Figure 2. 1 Sequence Alignment of ETH peptides from several insect species. Heavily conserved residues across species appear in larger fonts.

2.1.3. G protein-coupled receptors as insecticidal targets

G protein-coupled receptors (GPCRs) are members of the largest membrane receptor family present in almost all eukaryotes (Perez, 2005). They represent a class of transmembrane proteins involved in cell signaling, contain seven-transmembrane domains and sense signals from extracellular molecules. Insect GPCRs are generally classified in four families: Rhodopsin-like GPCRs, Secretin receptor-like GPCRs, Metabotropic glutamate receptor-like GPCRs, and Atypical GPCRs (Bai et al., 2013). Though these receptors share many structural features including the seven-transmembrane motif, their functions are incredibly diverse. GPCRs play key roles in many physiological processes such as smell, taste, and behavioral regulation in insects. As such, insect development, reproduction, and metabolism also rely on signaling through these receptors. Markedly, many GPCRs including ecdysis triggering hormone receptor (ETHR) and burcicon receptor are involved in ecdysis behavior (Arkane et al., 2008; Loveall et al., 2010). Earlier studies have shown that disruption of this signaling system leads to significant developmental defects, reproduction arrest, and death in many insect species, including *Anopheles gambiae* (Park et al., 2002). The ETHR is a neuropeptide GPCR that exists as two splicing isoforms in *Anopheles gambiae*: ETHR isoform A (ETHR A), and ETHR isoform B. While structures of either ETHR isoforms have not been reported yet, studies show distinct functions for each form in *Drosophila melanogaster* and *Leptinotarsa decemlineata* among others (Shi et al., 2019; Shen et al., 2020). Upon action by ETH, ETHR A is involved in signaling at the prepupae stage and is essential for larva-pupa ecdysis through activation of the eclosion hormone, kinin, crustacean cardioactive peptide, and others (Kim et al., 2006; Diao et al., 2016). Conversely, ETHR B activation plays a key role in larva-pupa transition by acting as an inhibitory signal for suppression of the premature expression and

release of the bursicon hormone from bursicon neurons (Shen et al., 2020). These studies provide an opportunity for insecticide development that may target different ETHR isoforms with the goal of halting larvae development at specific developmental stages. The ETH receptor is an ideal insecticidal target system because it will allow for the identification of effective chemical insecticides that will significantly reduce selectivity toward mammals, and thus, understanding this system and elucidating ETH/ETHR interactions is crucial for insecticide development.

2.2. Materials and Methods

2.2.1. Peptide Synthesis

The 17-residue AgETH1 peptide (SESPGFFIKLSKSVPRI-NH2) was chemically prepared by automated protocols of stepwise solid-phase synthesis using the standard 9-fluorenylmethoxycarbonyl (Fmoc) chemistry and acquired from PepMic Ltd, Jiangsu, China. Following deprotection and cleavage, the peptide was purified to >95% purity using reverse-phase HPLC on a C18 column. The mass and purity of the peptide was confirmed by matrix-assisted-laser desorption time-of-flight (MALDI-TOF) mass spectroscopy analysis. The mass of the AgETH1 peptide determined by mass spectroscopy (1891.60 Da) was consistent with the mass calculated from the sequence (1891.24 Da).

2.2.2. Circular Dichroism

Circular Dichroism (CD) analysis was performed to predict the secondary structure of AgETH1 using a Jasco-8155 spectropolarimeter (JASCO, Tokyo, Japan) using a 0.1-cm path length cell over the 190 to 260 nm range as previously described (Soulages et al., 2001). The CD spectra were acquired at 25°C every 1nm, with a 2-second averaging time per point and a 1-nm band pass. The peptide samples (2μM) were prepared in water with increasing Trifluoroethanol (TFE) percentage (0, 10, 20, 30, 40 and 50%). The mean residue ellipticity was expressed as percent ellipticity.

2.2.3. Nuclear Magnetic Resonance Spectroscopy

The 1D and 2D ^{1}H-^{1}H NMR experiments were performed on a 11.75 Tesla Varian 500 MHz VNMRS system (Agilent technologies Inc., Palo Alto, CA), operating at a frequency of

499.84 MHz for protons. The NMR data were acquired at the Biomolecular NMR Core Facility in the department of Biochemistry and Molecular Biophysics at Kansas State University. The data acquisition was carried out using a 5mm cryogenic triple resonance inverse detection pulse field gradient probe at 25℃. Purified AgETH1 was dissolved in 650 µL of 30% deuterated TFE (TFE-d3) and 70% H2O reaching a concentration of 2mM. A total of 16 increments of 2K data points were recorded for the 2D ^{1}H-^{1}H Double Quantum Filtered Correlation Spectroscopy (DQF-COSY) (Rance et al., 1983) experiments whereas 2D ^{1}H-^{1}H Total Correlation Spectroscopy (TOCSY) (Bax et al ., 1985) and Nuclear Overhauser Effect Spectroscopy (NOESY) (Kumar et al., 1980) experiments were performed using 2000 t2 and 256 t1 data points with spectral width of 12 ppm in each dimension and 16 transients per increment. Spin-lock time of 80ms at B1 field strength of 7kHz was used for 2D ^{1}H-^{1}H TOCSY experiments using MLEV-17 pulse sequence (Bax et al ., 1985), and mixing times of 100, 300 and 500 ms were used for 2D ^{1}H-^{1}H NOESY experiments. All data sets were collected in hyper-complex phase-sensitive mode. When necessary, spectral resolution was enhanced by Lorentzian-Gaussian apodization. Solvent peak suppression was performed by preset method and the residual solvent peak was used as reference for chemical shifts assignments. NMR data processing was done using VnmrJ3. 2a (Agilent Technologies., Palo Alto, CA) and analyzed using Sparky software (Goddard et al., 2008). Side chain proton resonances were assigned as previously discussed (Schrag et al., 2017) by overlaying cross peaks in the TOCSY spectra with those in the NOESY spectra acquired under similar conditions. NOE cross peaks were classified as strong, medium, weak, or very weak intensity based on the number of contour lines observed.

2.2.4. Chemical Shifts Assignments and Structure Calculations

The proton chemical shift assignments were made using 2-dimensiontnal ^{1}H-^{1}H TOCSY spectra for intra-residue spin systems and 2D ^{1}H-^{1}H NOESY spectra for inter-residue connectivities (Wuthrich et al., 1983). A total of 147 distance constraints obtained from the NOESY spectrum were used for structure calculations. The distance constraint measurements were carried out using NOESY cross peak observed in spectra with mixing time of 500 ms and also appeared in spectra with mixing time of 100 ms. The cross peak intensities were classified as strong (1.8-2.7Å), medium (1.8-3.4 Å), weak (1.8- 4.0 Å), and very weak (1.8-5.0 Å). Upper distance limits for NOEs involving methyl protons and non-stereo specifically assigned methylene protons were corrected appropriately, by adding 1 Å to the constraints for center averaging (Wuthrich et al., 1983). The distance constraints obtained were then used to create initial peptide structures starting from extended structures using the Crystallography and NMR System (CNS), version 1.3 (Brunger et al., 1998), which uses both simulated annealing protocol and molecular dynamics to produce low-energy structures with minimum distance and geometry violations. Default parameters were used to generate 100 structures for the initial CNS run. A second round of calculations generated 20 structures, from which the 10 lowest energy structures with no restriction violations were selected and analyzed with VMD 1.9.3 (Humphrey et al., 1996).

2.2.5. Synthetic Peptides and Analogs

Peptide analogs based on the native AgETH1 sequence were designed and synthesized by Pepmic Co., Ltd. (Suzhou, China) at a purity of over 90% as described in Section 2.2.1. All

synthetic peptides were prepared as stock solutions at a concentration of 1mM in assay buffer as previously described (Nachman et al., 2009).

2.2.6. Cell Culture, Transfections, and Calcium Bioluminescence Reporter Assay

Functional activation of the AgETH1 receptors were carried out in mammalian cell culture systems involving a Chinese hamster ovary (CHO-WTA11) cell line stably expressing ETHR A or ETHR B isoforms. Cells were then prepared for the receptor functional assay as previously described (Li et al., 2011; Aikins et al., 2008; Jiang et al., 2014). Stocks of peptide variants of AgETH1 were used for the preparation of serial dilutions. Cells were loaded into each well of a 96-well plate containing different peptide analogs at various concentrations as well as negative control (assay media alone) and positive control wells (ATP). After injection of the cells, luminescence was measured. Calculations, including determination of EC50 values, were conducted from the dose-response curves obtained from three technical replicates.

.

2.3. Results and Discussion

2.3.1. CD data and preliminary structural analysis

Circular Dichroism data was acquired for the AgETH1 peptide at increasing concentration of TFE in H2O at 25℃. As indicated on the CD spectrum shown in Figure 2.2, AgETH1 does not show considerable structure in pure water but shows two minima at ~205 and 225 nm once the TFE content in the sample exceeds 20%. These observed peaks on the CD spectrum are characteristics of alpha helices. As such, all further NMR experiments were conducted in 30% : 70% TFE-d3 : H2O solvent.

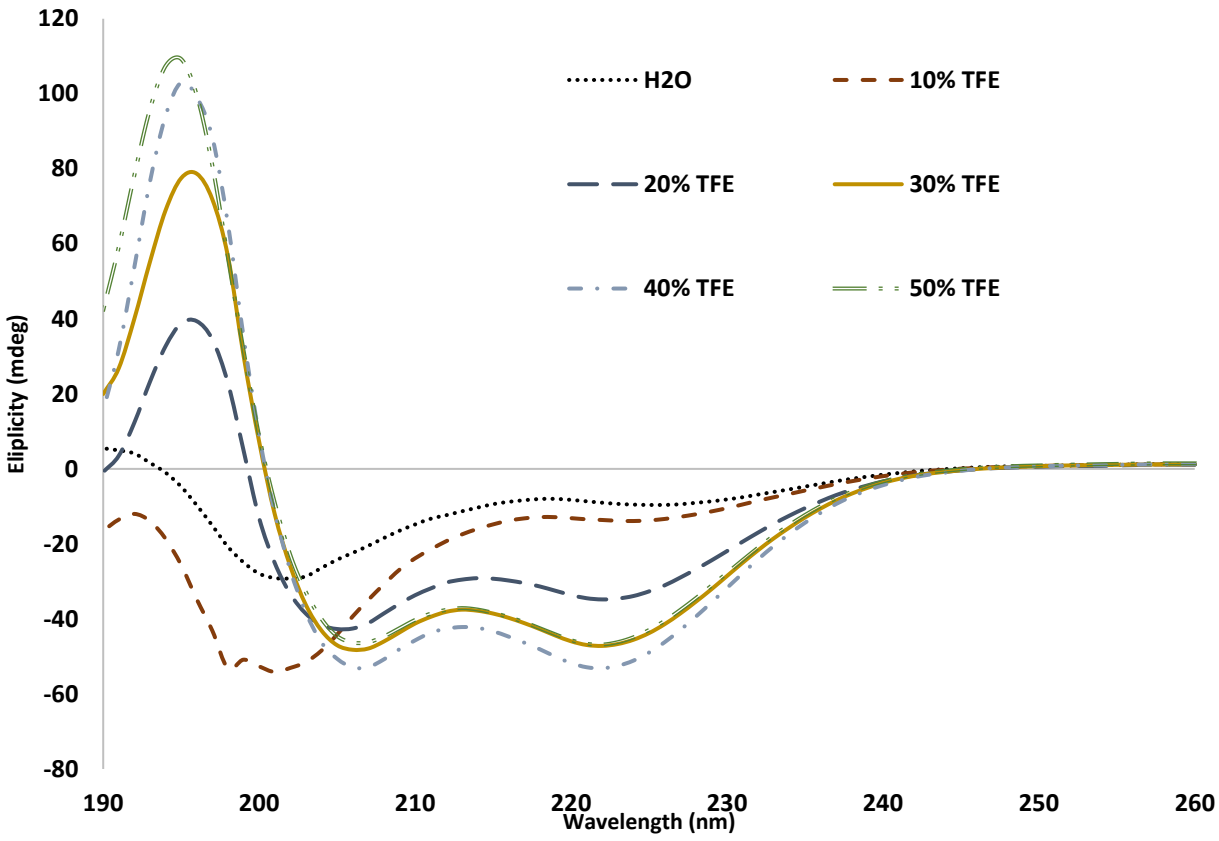

Figure 2. 2 Circular Dichroism data per v/v percent TFE concentration.

2.3.2. NMR results and peptide backbone conformation

2D ^{1}H-^{1}H TOCSY and NOESY NMR spectra acquired under similar experimental conditions were analyzed to identify the amino acid resonances and obtain proton chemical shift assignments. Figure 2.3 shows the NH-$C_{\alpha}H$, NH-$C_{\beta}H$, NH-$C_{\gamma}H$ and NH-$C_{\delta}H$ cross peak assignments in the fingerprint region of the 2D ^{1}H-^{1}H TOCSY spectrum used for residue identification of individual amino acid spin systems. Figure 2.4 illustrates 2D ^{1}H-^{1}H NOESY HN-HN region critical for secondary structural component determination.

.

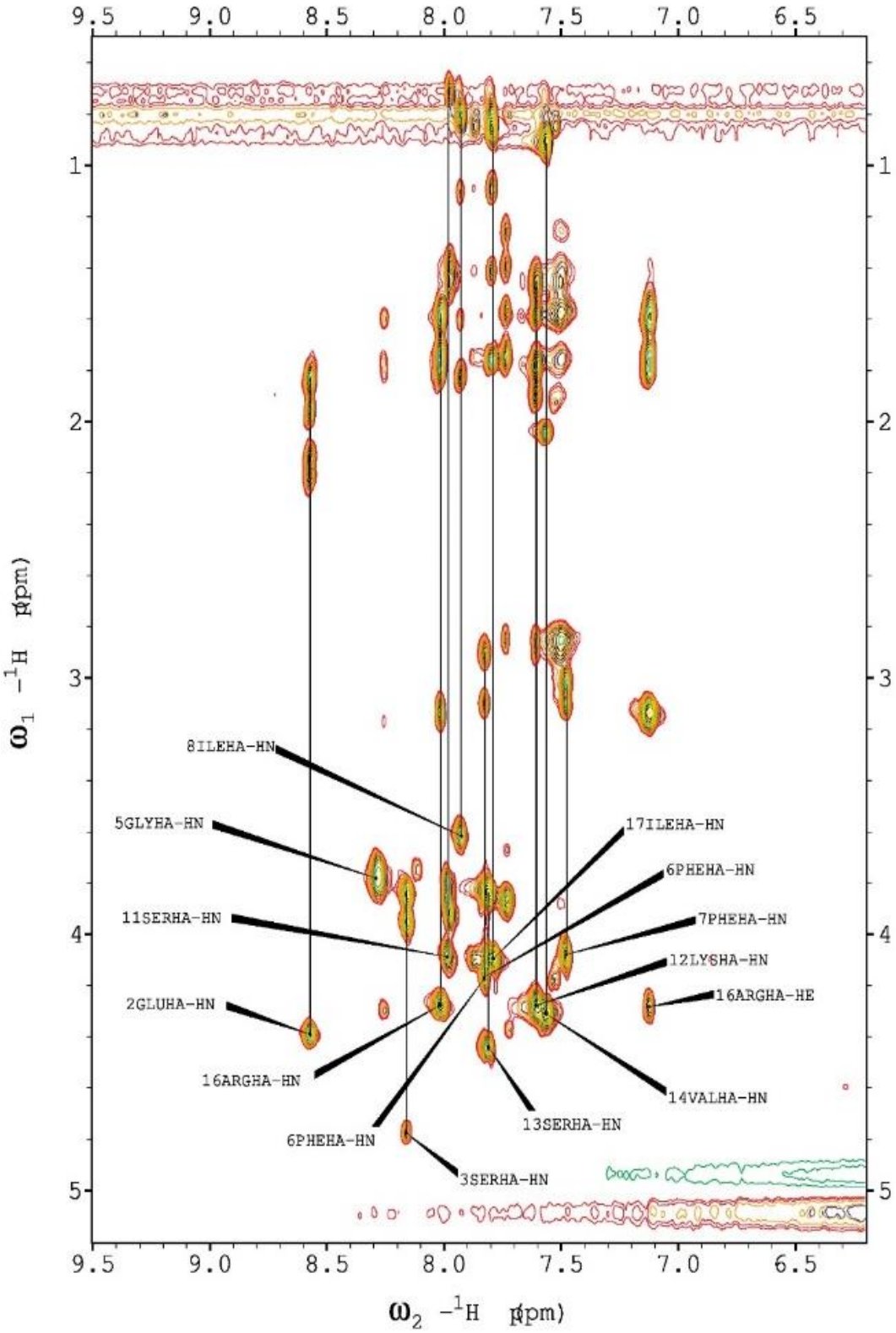

Figure 2. 3 2D ^{1}H-^{1}H TOCSY Fingerprint region representing NH-CαH, NH-CβH, NH-CγH and NH-CδH cross peaks.

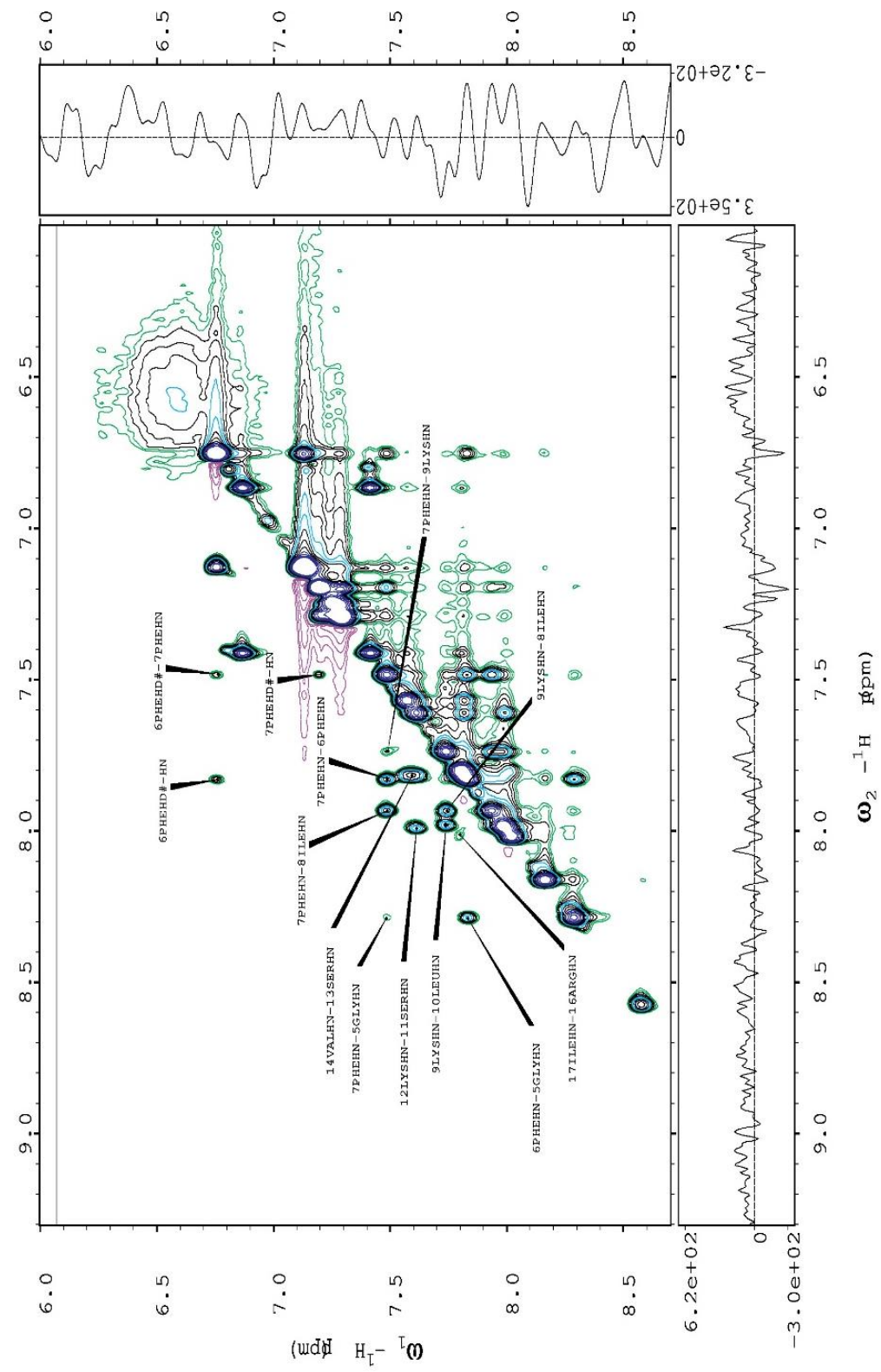

Figure 2. 4 2D ^{1}H-^{1}H NOESY HN-HN region.

Analysis of the 2D ^{1}H-^{1}H NOESY spectrum (Figure 2.4) allowed for the identification of $d_{\alpha N}(i, i+1)$ proton connectivities which were used for sequential assignments. Structural information was provided by the short, medium, and long range $d_{\alpha N}$ and d_{NN} connectivities which were obtained through further examination of the NOESY spectrum. Sequential d_{NN} NOEs, characteristic of alpha helices, were observed between residues 6F-7F, 7F-8I, 8I-9K, 9K-10L, 11S-12K, 13S-14V and 16R-17I (Figure 2.4). Table 2.1 shows the ^{1}H chemical shifts assignments for AgETH1 in 30% TFE-d3:70% H2O. The sequential, medium range and long range NOE connectivites are summarized in Figure 2.5.

Table 2. 1 AgETH1 Proton Chemical Shift (ppm) Assignments.

Column1	HN	HA	HB	HD and others
1SER	-	3.99	3.80	-
2GLU	8.48	4.31	2.10, 1.76	-
3SER	8.07	4.69	3.86, 3.76	-
4PRO	-	4.27	2.22	**δH** 3.74, 3.82 **γH** 1.94, 1.82
5GLY	8.20	3.69	-	-
6PHE	7.74	4.07	3.01, 2.82	-
7PHE	7.39	4.00	3.01, 2.93	-
8ILE	7.84	3.53	1.75	**δH** 0.72 **γH** 1.53, 1.02
9LYS	7.65	3.79	1.66, 1.18	**δH** 1.49 **γH** 1.31 **εH** 2.76
10LEU	7.89	3.84	1.38	**γH** 1.39 **δH** 0.63
11SER	7.90	3.99	3.70	-
12LYS	7.52	4.23	1.81, 1.69	**δH** 1.49 **γH** 1.37 **εH** 2.78
13SER	7.73	4.37	3.75	-
14VAL	7.48	4.23	1.96	**γH** 0.82
15PRO	-	4.26	2.12	**δH** 3.70, 3.49 **γH** 1.84
16ARG	7.93	4.19	1.68	**δH** 3.05 **γH** 1.51 **εH** 7.07
17ILE	7.71	4.01	1.67	**δH** 1.01 **γH** 1.33, 0.76

The absence of a dαα (i, i+1) NOE connectivity for prolines 4 and 15 and their corresponding preceding residues suggest that P4 and P15 adopted the trans conformation. The d_{NN} (i, i+1) sequential NOE connectivities (Figure 2.4) for residues 6-12 suggest that AgETH1 adopts a helical conformation in TFE:H2O (30:70) solution.

Table 2. 2 Structural statistics of the 10 Lowest Energy Structures of AgETH1 peptide.

NOE Constraints	Number
Total	147
Intra-residue	84
Sequential	44
Medium range	16
Long range	3
Constraints per residue	8.65
Pairwise RMSD to mean structure (residues 1-17)	
Backbone	1.99 ±0.55
Heavy Atoms	2.48 ±0.75
Pairwise RMSD to mean structure (residues 3-11)	
Backbone	1.86 ±0.65
Heavy Atoms	2.38 ±0.95
Percentage of residues in φ-ψ region	
Allowed	75.82
Additionally Allowed	19.17
Generously Allowed	4.15
Disallowed	0.83

For structural calculations, a total of 147 NOE distance constraints including 84 intra-residue, 44 sequential, 16 medium range and 3 long range constraints were used (Table 2.2). From the initial 100 structures generated, the 10 lowest energy structures were retained. Superimposition of the 10 lowest energy structures showed considerable degree of rigidity with a pairwise root mean square deviation of the backbone of 1.99 Å (Table 2.2). Alignment along residues 3-11 of the 10 lowest energy structures showed similar rigidity with a backbone root mean square deviation of 1.86 Å (Table 2.2). The average structure of the 10 lowest energy structures was considered as the NMR solution structure for AgETH1 peptide. This structure is comprised of a short alpha helix between residues 3S and 11S while the N and C terminal regions are largely unstructured (Figure 2.6).

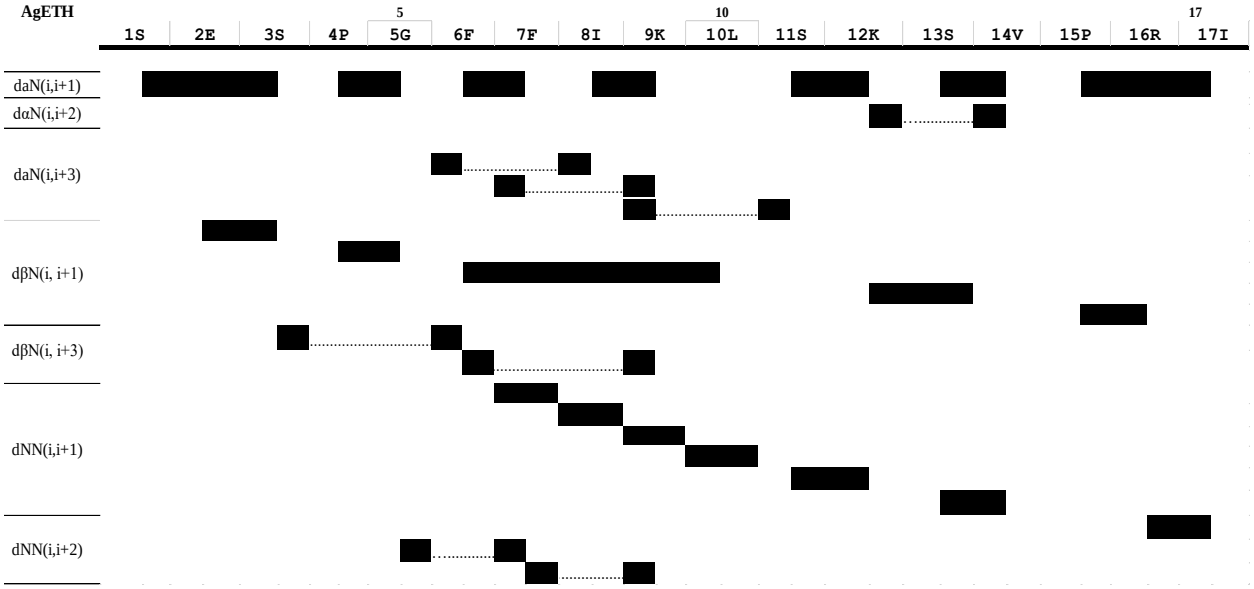

Figure 2. 5 Summary of NOE connectivities obtained for AgETH1 in 30% TFE.

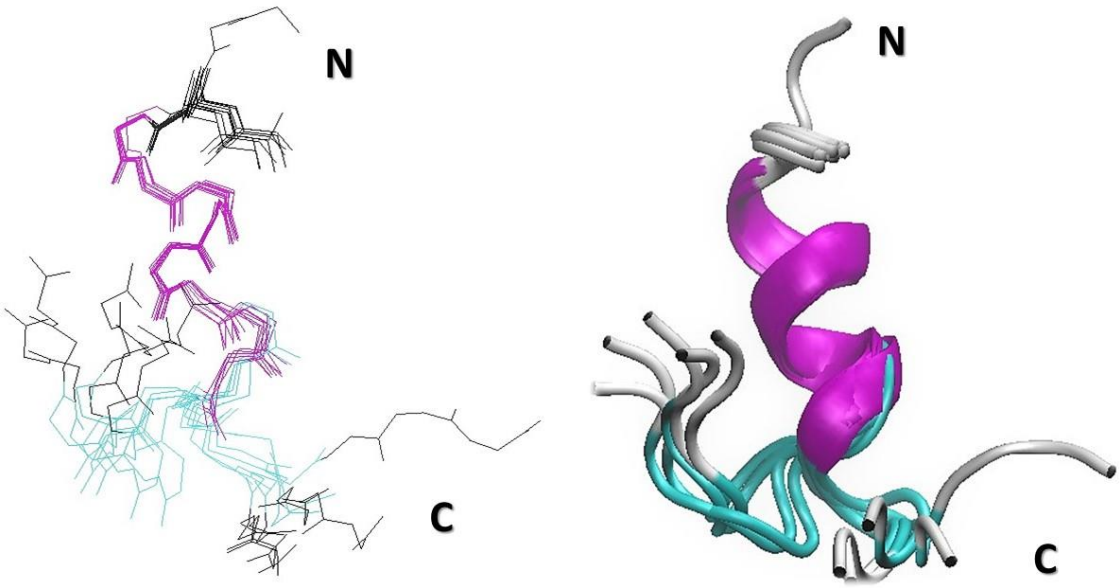

Figure 2. 6 Structural Representation of AgETH1 in 30% TFE.

2.3.3. Synthetic and wild type AgETH1 activity on ETHR A

To assess the biological implications of the alpha helical structure of wild type AgETH1, seven synthetic variants of AgETH1 containing mutations and truncations at various highly conserved residue positions were generated. The functional activation of ETHR-A by these variants was evaluated via a Calcium bioluminescence reporter assay. The sequences of the variants and the EC50 values obtained from the activity assay are presented in Table 2.3. As shown by the EC50 values obtained (Table 2.3), and the dose response curves measured for each variant (Figure 2.7), retention of the C-terminal PRXamide motif is critical for receptor activation. AgETH1 variants lacking the N-terminal region (AgETH1-12, -9, -6) retain activity. The assays also show retention of peptide activity akin to WT for the variant K9A while the truncated peptides AgETH1-6 K12A show decreased activity in comparison to WT (Figure 2.7). AgETH1-12 and F7A show enhanced activity when compared to WT, suggesting that the N-terminal region of the peptide may not be important for activity since the truncated peptides containing the core region as well as the C-terminus show conservation (K9A) or enhancement (AgETH-12, F7A) of peptide activity in comparison to WT. Additionally, mutations preserving the heavily conserved Lysine residue at position 12 (AgETH1-12, K9A, F7A) show retention of peptide activity with the exception of AgETH1-9. Mutation at residue position 12 shows a drastic decrease in peptide activity, suggesting that this residue position may be crucial for receptor activation. Overall, these results suggest that the N-terminal region is not crucial for receptor activation by AgETH1 and that the second highly conserved Lysine residue (K12) plays a more important role than K9.

Table 2. 3 EC50 values for the wild type AgETH1 peptide and synthetic analogs.

Peptide/ Analog	Analog Sequence	nM EC50 – AgETHR A
AgETH1 WT	SESPGFFI**K**LS**K**SV**PR**I-NH2	438
AgETH1 F7A	SESPGF**A**IKLSKSV**PR**I-NH2	963
AgETH1 K9A	SESPGFFI**A**LSKSV**PR**I-NH2	1800
AgETH1 K12A	SESPGFFI**K**LS**A**SV**PR**I-NH2	3327
AgETH1 12	FFI**K**LS**K**SV**PR**I-NH2	482
AgETH1 9	**K**LS**K**SV**PR**I-NH2	1726
AgETH1 6	**K**SV**PR**I-NH2	2922
AgETH1 6 K12A	**A**SV**PR**I-NH2	3667

EC50 values represent the average of three technical replicates. Heavily conserved residues appear in bold font colored in black. Point mutation positions appear in bold font colored in red.

To investigate the role of the previously determined NMR solution structure of AgETH1 in receptor activation by this peptide, circular dichroism experiments were performed on AgETH1 WT, and variants AgETH1-12, K9A, and K12A. The CD experimental data (Figure 2.4) show retention of the helical structure for both mutants K9A and K12A, while the truncated peptide, AgETH1-12 shows a largely unstructured conformation in solution. These results suggest that the alpha helical conformation previously obtained is not crucial for receptor activation but may be important to enhance the structural stability of the AgETH1 peptide *in vivo*.

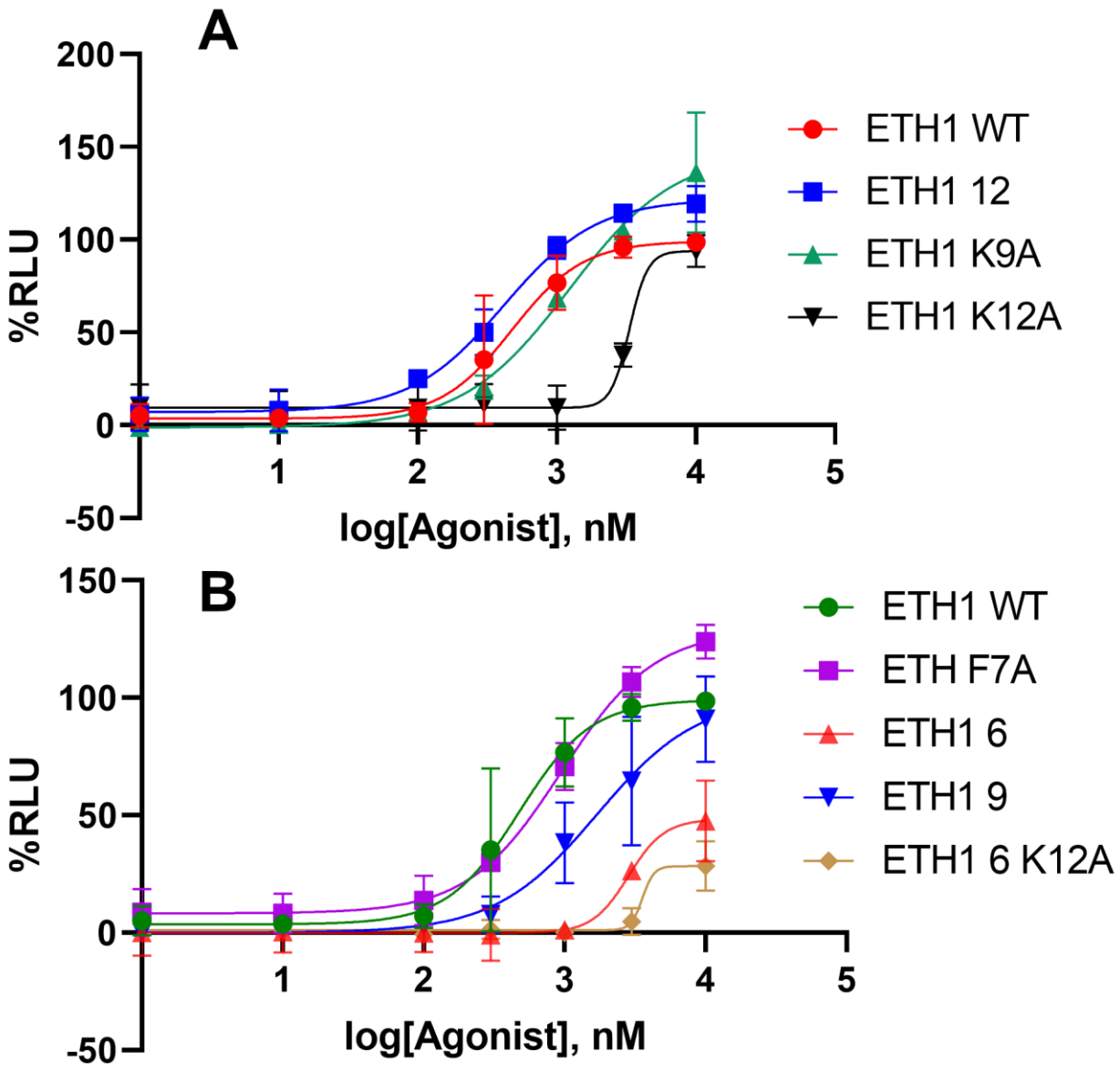

Figure 2. 7 Dose response curves of AgETH1 mutants against AgETHR A.

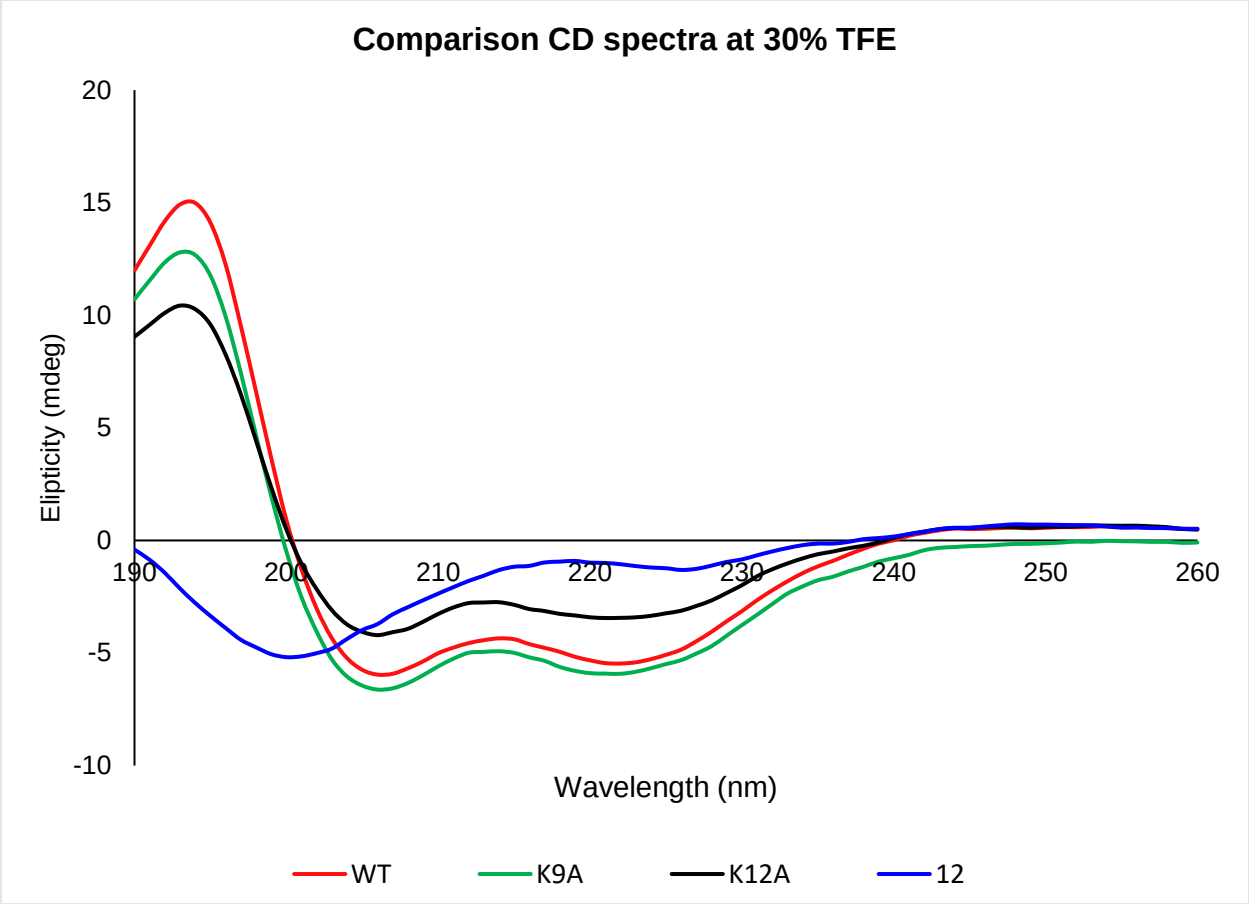

Figure 2. 8 Circular Dichroism data at 30 percent TFE concentration of AgETH1 WT and mutants.

2.4. Conclusions

The ecdysis process in insects is one that involves highly complex hormonal signaling and results in a multitude of behavioral events that are crucial to insect larval development. The effector hormone of this process, ETH, is a 17 amino acid long neuropeptide released by Inka cells and acts on neuropeptide G protein-coupled receptors. These receptors provide great targets for the development of future insecticides with reduced selectivity against mammals. It is therefore of importance to understand the receptor-ligand interactions that mediate ecdysis signaling. In this study, we have determined the NMR solution structure of AgETH1 and provided insight into specific residue positions that are crucial for receptor activation. Mature AgETH1 is comprised of a short alpha helix between residues 3S and 11S. Subsequent investigation into the role of highly conserved residue positions in AgETH1 showed that the C-terminal region of the peptide is crucial for receptor activation, as previously described (Zitnan et al., 2005). The activity assays also suggest that one of the two heavily conserved Lysine residues (K12) may play a more important role in receptor activation than the other (K9). These results led to the investigation of the role of the alpha helical structure upon receptor activation by AgETH1 through circular dichroism experiments. The CD experimental data show retention of the helical structure for both mutants K9A and K12A, while the truncated peptide, ETH-12 shows a largely unstructured conformation in solution. These results suggest that the alpha helical conformation previously obtained is not crucial for receptor activation but may be important to enhance the structural stability of the AgETH1 peptide *in vivo*. In addition to these findings, our studies also show that the N-terminal region of AgETH1 is not crucial for receptor activation as was suggested by the highly conserved phenylalanine residues at positions 6 and 7. Though the roles of the alpha helical structure of the core region and the

extended N-terminal conserved residues remain unclear, it is probable that these features exist to enhance the peptide's structural stability and facilitate interactions with the receptor, AgETHR. In particular, the two conserved phenylalanine residues at positions 6 and 7 may facilitate interactions with membrane lipids due to their hydrophobic nature as the peptide finds its way to the membrane-integrated receptor *in vivo*.

2.5. References

Aikins, M. J., Schooley, D. A., Begum, K., Detheux, M., Beeman, R. W., & Park, Y. (2008). Vasopressin-like peptide and its receptor function in an indirect diuretic signaling pathway in the red flour beetle. *Insect Biochemistry and Molecular Biology*, *38*(7), 740–748.

Aktar, W., Sengupta, D., & Chowdhury, A. (2009). Impact of pesticides use in agriculture: Their benefits and hazards. *Interdisciplinary Toxicology*, *2*(1), 1–12.

Arakane, Y., Li, B., Muthukrishnan, S., Beeman, R. W., Kramer, K. J., & Park, Y. (2008). Functional analysis of four neuropeptides, EH, ETH, CCAP and bursicon, and their receptors in adult ecdysis behavior of the red flour beetle, Tribolium castaneum. *Mechanisms of Development*, *125*(11–12), 984–995.

Areiza, M., Nouzova, M., Rivera-Perez, C., & Noriega, F. G. (2014). Ecdysis triggering hormone ensures proper timing of juvenile hormone biosynthesis in pharate adult mosquitoes. *Insect Biochemistry and Molecular Biology*, *54*, 98–105.

Bai, H., & Palli, S. R. (2010). Functional characterization of bursicon receptor and genome-wide analysis for identification of genes affected by bursicon receptor RNAi. *Developmental Biology*, *344*(1), 248–258.

Bai, H., & Palli, S. R. (2013). G protein-coupled receptors as target sites for insecticide discovery. In *Advanced Technologies for Managing Insect Pests*, 57–82.

Bax, A., & Davis, D. G. (1985). MLEV-17-based two-dimensional homonuclear magnetization transfer spectroscopy. *Journal of Magnetic Resonance (1969)*, *65*(2), 355–360.

Brünger, A. T., Adams, P. D., Clore, G. M., Delano, W. L., Gros, P., Grossekunstleve, R. W., Jiang, J. S., Kuszewski, J., Nilges, M., Pannu, N. S., Read, R. J., Rice, L. M., Simonson, T., & Warren, G. L. (1998). Crystallography & NMR system: A new software suite for macromolecular structure determination. *Acta Crystallographica Section D: Biological Crystallography*, *54*(5), 905–921.

Campbell-Lendrum, D., Manga, L., Bagayoko, M., & Sommerfeld, J. (2015). Climate change and vector-borne diseases: What are the implications for public health research and policy? *Philosophical Transactions of the Royal Society B: Biological Sciences*, *370*(1665), 1–8.

Dai, H., Ma, L., Wang, J., Jiang, R., Wang, Z., & Fei, J. (2008). Knockdown of ecdysis-triggering hormone gene with a binary *UAS/GAL4* RNA interference system leads to lethal ecdysis deficiency in silkworm. *Acta Biochimica et Biophysica Sinica*, *40*(9), 790–795.

Dai, L., & Adams, M. E. (2009). Ecdysis triggering hormone signaling in the yellow fever mosquito Aedes aegypti. *General and Comparative Endocrinology*, *162*(1), 43–51.

Diao, F., Mena, W., Shi, J., Park, D., Diao, F., Taghert, P., Ewer, J., & White, B. H. (2016). The splice isoforms of the Drosophila ecdysis triggering hormone receptor have developmentally distinct roles. *Genetics*, *202*(1), 175–189.

Goddard, T. D., & Kneller, D. G. (2008). Sparky 3. University of California, San Francisco, USA 15 (20).

Humphrey, W., Dalke, A., & Schulten, K. (1996). VMD: Visual molecular dynamics. *Journal of Molecular Graphics*, *14*(1), 33–38.

Jiang, H., Wei, Z., Nachman, R. J., & Park, Y. (2014). Molecular cloning and functional characterization of the diapause hormone receptor in the corn earworm Helicoverpa zea. *Peptides*, *53*, 243–249.

Kataoka, H., Troetschler, R. G., Kramer, S. J., Cesarin, B. J., & Schooley, D. A. (1987). Isolation and primary structure of the eclosion hormone of the tobacco hornworm, Manduca sexta. *Biochemical and Biophysical Research Communications*, *146*(2), 746–750.

Kim, Y. J., Žitňan, D., Cho, K. H., Schooley, D. A., Misoguchi, A., & Adams, M. E. (2006).

Central peptidergic ensembles associated with organization of an innate behavior. *Proceedings of the National Academy of Sciences of the United States of America*, *103*(38), 14211–14216.

Kim, Y. J., Žitňan, D., Galizia, C. G., Cho, K. H., & Adams, M. E. (2006). A Command Chemical Triggers an Innate Behavior by Sequential Activation of Multiple Peptidergic Ensembles. *Current Biology*, *16*(14), 1395–1407.

Kumar, A., Ernst, R. R., & Wüthrich, K. (1980). A two-dimensional nuclear Overhauser enhancement (2D NOE) experiment for the elucidation of complete proton-proton cross-relaxation networks in biological macromolecules. *Topics in Catalysis*, *95*(1), 1–6.

Lenaerts, C., Cools, D., Verdonck, R., Verbakel, L., Vanden Broeck, J., & Marchal, E. (2017). The ecdysis triggering hormone system is essential for successful moulting of a major hemimetabolous pest insect, Schistocerca gregaria. *Scientific Reports*, *7*(1), 1–14.

Li, B., Beeman, R. W., & Park, Y. (2011). Functions of duplicated genes encoding CCAP receptors in the red flour beetle, Tribolium castaneum. *Journal of Insect Physiology*, *57*(9), 1190–1197.

Loveall, B. J., & Deitcher, D. L. (2010). The essential role of bursicon during drosophila development. *BMC Developmental Biology*, *10*(1), 1–17.

Marti, T., Takio, K., Walsh, K. A., Terzi, G., & Truman, J. W. (1987). Microanalysis of the amino acid sequence of the eclosion hormone from the tobacco hornworm *Manduca sexta*. *FEBS Letters*, *219*(2), 415–418.

Meiselman, M. R., Kingan, T. G., & Adams, M. E. (2018). Stress-induced reproductive arrest in Drosophila occurs through ETH deficiency-mediated suppression of oogenesis and ovulation. *BMC Biology*, *16*(1), 18.

Nachman, R. J., Ben Aziz, O., Davidovitch, M., Zubrzak, P., Isaac, R. E., Strey, A., Reyes-Rangel, G., Juaristi, E., Williams, H. J., & Altstein, M. (2009). Biostable β-amino acid PK/PBAN analogs: Agonist and antagonist properties. *Peptides*, *30*(3), 608–615.

Nyati, P., Nouzova, M., Rivera-Perez, C., Clifton, M. E., Mayoral, J. G., & Noriega, F. G. (2013). Farnesyl Phosphatase, a Corpora allata Enzyme Involved in Juvenile Hormone Biosynthesis in Aedes aegypti. *PLoS ONE*, *8*(8).

Park, Y., Kim, Y. J., & Adams, M. E. (2002). Identification of G protein-coupled receptors for Drosophila PRXamide peptides, CCAP, corazonin, and AKH supports a theory of ligand-receptor coevolution. *Proceedings of the National Academy of Sciences of the United States of America*, *99*(17), 11423–11428.

Park, Y., Kim, Y. J., Dupriez, V., & Adams, M. E. (2003). Two subtypes of ecdysis-triggering

hormone receptor in Drosophila melanogaster. *Journal of Biological Chemistry*, *278*(20), 17710–17715.

Park, Y., Zitnan, D., Gill, S. S., & Adams, M. E. (1999). Molecular cloning and biological activity of ecdysis-triggering hormones in Drosophila melanogaster. *FEBS Letters*, *463*(1–2), 133–138.

Perez, D. M. (2005). From plants to man: The GPCR "tree of life." In *Molecular Pharmacology* (Vol. 67, Issue 5, pp. 1383–1384). American Society for Pharmacology and Experimental Therapeutics.

Rance, M., Sørensen, O. W., Bodenhausen, G., Wagner, G., Ernst, R. R., & Wüthrich, K. (1983). Improved spectral resolution in COSY 1H NMR spectra of proteins via double quantum filtering. *Biochemical and Biophysical Research Communications*, *117*(2), 479–485.

Ranson, H., & Lissenden, N. (2016). Insecticide Resistance in African Anopheles Mosquitoes: A Worsening Situation that Needs Urgent Action to Maintain Malaria Control. In *Trends in Parasitology* (Vol. 32, Issue 3, pp. 187–196). Elsevier Ltd.

Shen, C. H., Xu, Q. Y., Fu, K. Y., Guo, W. C., Jin, L., & Li, G. Q. (2020). Two Splice Isoforms of Leptinotarsa Ecdysis Triggering Hormone Receptor Have Distinct Roles in Larva-Pupa Transition. *Frontiers in Physiology*, *11*.

Schrag, L. G, Cao, X., I. Herrera, A., Wang, Y., Jiang, H., & Prakash, O. (2017). Solution Structure and Expression Profile of an Insect Cytokine: *Manduca sexta* Stress Response Peptide-2. *Protein and Peptide Letters*, *24*(1), 3–11.

Shi, Y., Jiang, H.-B., Gui, S.-H., Liu, X.-Q., Pei, Y.-X., Xu, L., Smagghe, G., & Wang, J.-J. (2017). Ecdysis Triggering Hormone Signaling (ETH/ETHR-A) Is Required for the Larva-Larva Ecdysis in Bactrocera dorsalis (Diptera: Tephritidae). *Frontiers in Physiology*, *8*(AUG), 587.

Shi, Y., Liu, T.-Y., Jiang, H.-B., Liu, X.-Q., Dou, W., Park, Y., Smagghe, G., & Wang, J.-J. (2019). The Ecdysis Triggering Hormone System, via ETH/ETHR-B, Is Essential for Successful Reproduction of a Major Pest Insect, Bactrocera dorsalis (Hendel). *Frontiers in Physiology*, *10*(3), 151.

Soulages, J. L., Arrese, E. L., Chetty, P. S., & Rodriguez, V. (2001). Essential Role of the Conformational Flexibility of Helices 1 and 5 on the Lipid Binding Activity of Apolipophorin-III. *Journal of Biological Chemistry*, *276*(36), 34162–34166.

Truman, J. W. (1971). PHYSIOLOGY OF INSECT ECDYSIS I. THE ECLOSION BEHAVIOUR OF SATURNIID MOTHS AND ITS HORMONAL RELEASE. In *J. Exp. Biol* (Vol. 54).

Truman, J. W. (2005). Hormonal Control of Insect Ecdysis: Endocrine Cascades for Coordinating Behavior with Physiology. In *Vitamins and Hormones* (Vol. 73, pp. 1–30). Academic Press.

Truman, J. W., & Riddiford, L. M. (1970). Neuroendocrine control of ecdysis in silkmoths. *Science*, *167*(3925), 1624–1626.

Weeks, J. C., & Truman, J. W. (1984). Neural organization of peptide-activated ecdysis behaviors during the metamorphosis of Manduca sexta - I. Conservation of the peristalsis motor pattern at the larval-pupal transformation. *Journal of Comparative Physiology A*, *155*(3), 407–422.

Wüthrich, K., Billeter, M., & Braun, W. (1983). Pseudo-structures for the 20 common amino acids for use in studies of protein conformations by measurements of intramolecular proton-proton distance constraints with nuclear magnetic resonance. *Journal of Molecular Biology*, *169*(4), 949–961.

Žitňan, D., & Daubnerová, I. (2016). Ecdysis Triggering Hormone. In *Handbook of Hormones* (pp. 461-e77-3). Elsevier.

Žitňan, D., Žitňanová, I., Spalovská, I., Takáč, P., Park, Y., & Adams, M. E. (2003). Conservation of ecdysis-triggering hormone signaling in insects. *Journal of Experimental Biology, 206*(8), 1275–1289.

Žitňan, D., Kingan, T. G., Hermesman, J. L., & Adams, M. E. (1996). Identification of ecdysis-triggering hormone from an epitracheal endocrine system. *Science, 271*(5245), 88–91.